

GNAQPMS-Hg v1.0, a global nested atmospheric mercury transport model: Model description, evaluation and application to trans-boundary transport of Chinese anthropogenic emissions

**H. S. Chen¹, Z. F. Wang¹, J. Li¹, X. Tang¹, B. Z. Ge¹, X. L. Wu¹, O. Wild²,
and G. R. Carmichael³**

¹ LAPC, Institute of Atmospheric Physics, Chinese Academy of Sciences, Beijing, China

² Lancaster Environment Centre, Lancaster University, Lancaster, UK

³ Center for Global and Regional Environmental Research (CGRER), University of Iowa, Iowa City, Iowa, USA

Correspondence to: Z. F. Wang (zifawang@mail.iap.ac.cn)

1 **Abstract**

2 Atmospheric mercury (Hg) is a toxic pollutant and can be transported over the whole
3 globe due to its long lifetime in the atmosphere. For the purpose of assessing Hg
4 hemispheric transport and better characterizing regional Hg pollution, a global
5 nested atmospheric Hg transport model (GNAQPMS-Hg) has been developed. In
6 GNAQPMS-Hg, the gas and aqueous phase Hg chemistry representing the
7 transformation among three forms of Hg: elemental mercury (Hg(0)), divalent
8 mercury (Hg(II)), and primary particulate mercury (Hg(P)) are calculated. A detailed
9 description of the model, including mercury emissions, gas and aqueous phase
10 chemistry, and dry and wet deposition is given in this study. Worldwide observations
11 including extensive data in China have been collected for model evaluation.
12 Comparison results show that the model reasonably simulates the global mercury
13 budget and the spatial-temporal variation of surface mercury concentrations and
14 deposition. Overall, model predictions of annual total gaseous mercury (TGM) and
15 wet deposition agree with observations within a factor of two, and within a factor of
16 five for oxidized mercury and dry deposition. The model performs significantly
17 better in North America and Europe than in East Asia. This can probably be
18 attributed to the large uncertainties in emission inventories, coarse model resolution
19 and to the inconsistency between the simulation and observation periods in East Asia.
20 Compared to the global simulation, the nested simulation shows improved skill at
21 capturing the high spatial variability of surface Hg concentrations and deposition
22 over East Asia. In particular, the root mean square error (RMSE) of simulated Hg
23 wet deposition over East Asia is reduced by 24% in the nested simulation. Model
24 sensitivity studies indicate that Chinese primary anthropogenic emissions account
25 for 30% and 62% of surface mercury concentrations and deposition over China,
26 respectively. Along the rim of the western Pacific, the contributions from Chinese
27 sources are 11% and 15.2% over the Korean Peninsula, 10.4% and 8.2% over
28 Southeast Asia, and 5.7% and 5.9% over Japan. But for North America, Europe and
29 West Asia, the contributions from China are all below 5%.

1 **1 Introduction**

2 Since the Minamata Event in Japan in the 1960s (Harada, 1995), the toxicity of
3 mercury (Hg) on human health and the environment has caused widespread public
4 concern. Hg is a persistent, bio-accumulated pollutant, and the only heavy metal that
5 can be transported globally in gaseous form (Schroeder and Munthe, 1998). As a
6 result, Hg has been listed as a priority pollutant by many countries and international
7 agencies. After a long struggle, the first global treaty (the Minamata Convention)
8 aimed at reducing Hg emissions and releases, was adopted and signed by 92 countries
9 in 2013 (<http://www.mercuryconvention.org/>). This made an important advance
10 towards joint action to control global Hg pollution and has brought higher
11 requirements for understanding global Hg source-receptor relationships, especially the
12 impacts of high regional emissions (e.g. from China and India) on global Hg levels.
13 However, besides the remaining uncertainties in emission estimates, poor
14 understanding of the chemical transformation of atmospheric mercury has made
15 assessment of long-range transport very challenging (AMAP/UNEP, 2013).

16 Atmospheric mercury models are powerful tools to assess the fate and transport of
17 mercury in the atmosphere. A number of atmospheric mercury models have been
18 developed to investigate the emissions, transport, chemistry, deposition and
19 source-receptor relationships of Hg at global and regional scales. Global models
20 include the GEOS-Chem model (Amos et al., 2012; Zhang et al., 2012), the CTM-Hg
21 model (Seigneur et al., 2004), the CAM-Chem-Hg model (Lei et al., 2013), the
22 ECHMERIT model (De Simone et al., 2014), the MSCE-Hg-Hem model (Travnikov
23 and Ilyin, 2009), the DEHM model (Christensen et al., 2004), and the GRAHM model
24 (Dastoor and Durnford, 2014). Regional models include the CMAQ-Hg model (Bash,
25 2010), the STEM-Hg model (Pan et al., 2008), the CAMx-Hg model (ENVIRON,
26 2011) and the WRF-Chem-Hg model (Gencarelli et al., 2014). Application of these
27 models has greatly advanced our understanding of the global Hg cycle. However,
28 several model intercomparison studies (Ryaboshapko et al., 2007; Bullock et al., 2008;
29 Pirrone and Keating, 2010) have found that large uncertainties still exist in Hg models

1 and there is much room for improvement, especially for simulation of reactive
2 gaseous mercury (RGM) and dry deposition.

3 Mercury is released to the atmosphere from both anthropogenic and natural sources.
4 Human activities have increased the amount of mercury cycling through the
5 atmosphere-ocean-terrestrial system by about a factor of three (Selin, 2009), although
6 anthropogenic sources are estimated to account for only 31% of total Hg emissions
7 (Pirrone et al., 2010). China has the world's largest Hg production, consumption and
8 emissions, and suffers the most serious Hg pollution (Jiang et al., 2006), but the
9 impacts of its anthropogenic emissions on global Hg levels are still unclear. Previous
10 modeling studies mainly focused on long-range transport of mercury from Asia.
11 Based on the GEOS-Chem model, about 7-20% of Hg deposition over the United
12 States (US) was found to originate from Asian anthropogenic sources, which was
13 comparable to that from North American sources (Strode et al., 2008; Jaffe and Strode,
14 2008). Another modeling study using the CTM-Hg model with three emission
15 scenarios indicated that Asian anthropogenic emissions accounted for 14–25% of Hg
16 deposition over the US (Seigneur et al., 2004). Travnikov (2005) reported a
17 contribution to Hg deposition from total Asian sources (including both anthropogenic
18 and natural emissions) of 15% over Europe and 33% over the Arctic. Corbitt et al.
19 (2011) further pointed out that Asian emissions are the largest contributors to
20 anthropogenic deposition to all ocean basins and these contributions are expected to
21 further grow in the future. The above studies all treated Asian anthropogenic
22 emissions as a whole, and the effects of anthropogenic emissions from the world's
23 largest single emitter (China) have not been explicitly assessed before. In addition,
24 due to lack of observational data, little model validation has been conducted over East
25 Asia (especially China) in these studies and this leads to greater uncertainty in the
26 conclusions. Fu et al. (2012) reviewed previous modeling studies and pointed out that
27 current model simulations tend to underestimate total gaseous mercury (TGM) and
28 total particulate mercury (TPM) concentrations but overestimate reactive gaseous
29 mercury (RGM) concentrations in China. To improve Hg model skill in China, nested
30 simulations with high horizontal resolution might be a good choice. Zhang et al. (2012)

1 demonstrated that a nested-grid model can capture the variation of Hg wet deposition
2 over North America better than a global model. In this study, online nested Hg
3 simulation with flexible horizontal resolution was developed and evaluated.
4 Compared to traditional multi-scale modeling approach (using a global model to
5 provide initial and boundary conditions to a regional model) (Seigneur et al., 2001),
6 online nested method use the same physical and chemical parameterizations in the
7 global and nested domains which could avoid uncertainties induced by different
8 boundary conditions. Compared to offline nested method used in the GEOS-Chem
9 model (Zhang et al., 2012), online nested method can provide boundary conditions
10 with higher time resolution (10 or 5 minutes) from the global domain to the nested
11 domain. Hence, online nested simulation would potentially improve model
12 performance in regional scale.

13 Therefore, a comprehensive evaluation and improvement of Hg model performance
14 in China is needed to effectively reduce the uncertainties in Hg trans-boundary
15 transport and a quantitative assessment of Chinese anthropogenic contribution to
16 global Hg concentration and deposition levels is helpful to determine and fulfill the
17 Hg emission reduction tasks under the Minamata Convention.

18 In this paper, we describe the development of a global nested atmospheric mercury
19 transport model (GNAQPMS-Hg) incorporating the latest available physical and
20 chemical processes essential to the mercury life cycle. The spatial and temporal
21 variability of Hg concentrations and deposition are comprehensively evaluated against
22 available worldwide observations, including extensive data from China. The impact of
23 horizontal resolution ($1^{\circ}\times 1^{\circ}$ in the global domain versus $0.33^{\circ}\times 0.33^{\circ}$ in the nested
24 domain) on model predictions over East Asia is examined. Finally, the trans-boundary
25 transport of Chinese primary anthropogenic Hg emissions is quantified using the
26 model.

1 **2 Model description and setup**

2 **2.1 General description**

3 The atmospheric physics and chemistry component of GNAQPMS-Hg, with the
4 exception of the mercury module, is based on the Nested Air Quality Prediction
5 Modeling System (NAQPMS) (Wang et al., 2006), developed at the Institute of
6 Atmospheric Physics, Chinese Academy of Sciences. NAQPMS is a 3-D regional
7 Eulerian model which has been rigorously evaluated and widely applied to simulate
8 the chemical evolution and transport of ozone (Li et al., 2007; Tang et al., 2010), the
9 distribution and evolution of aerosol and acid rain over East Asia (Wang et al., 2002;
10 Li et al., 2011; Li et al., 2012) and to provide operational air quality forecasts in mega
11 cities such as Beijing, Shanghai and Guangzhou (Wang et al., 2010; Wu et al., 2012;
12 Wang et al., 2009). GNAQPMS is the global version of NAQPMS and uses the same
13 model framework and physical and chemical parameterization schemes.

14 As a multi-scale model, GNAQPMS can simulate the transportation and formation
15 of primary and secondary pollutants from urban to global scale using an online
16 nesting approach. It includes advection, diffusion and convection processes,
17 gas/aqueous/aerosol chemistry, and modules for dry and wet deposition. The
18 advection process is parameterized based on an accurate mass conservative,
19 peak-preserving algorithm provided by Walcek and Aleksic (1998). The gas phase
20 chemical mechanism is the CBM-Z mechanism (Zaveri and Peters, 1999), including
21 133 reactions for 53 species. The dry deposition module uses the parameterization of
22 Wesely (1989). The wet deposition and aqueous-phase chemistry module is
23 constructed based on a revised version of the RADM mechanism (Chang et al., 1987;
24 Wang et al., 2002; Ge et al., 2014). A mercury module has been developed and
25 coupled into the GNAQPMS model in this study, as described in Sect. 2.2 to 2.4.
26 Hereafter, we call this new model GNAQPMS-Hg. Note that meteorology, emissions,
27 deposition and chemistry are self-consistent between the global and nested domains.

1 **2.2 Mercury chemistry**

2 **2.2.1 Basic mechanism**

3 In GNAQPMS-Hg, three forms of mercury are explicitly treated: elemental mercury
4 (Hg(0)), divalent mercury (Hg(II)), and primary particulate mercury (Hg(P)).
5 Transformations between these three forms include the gas phase oxidation of Hg(0)
6 to Hg(II), the aqueous phase oxidation of Hg(0) to Hg(II), the aqueous phase
7 reduction of Hg(II) to Hg(0), the aqueous phase equilibria of Hg(II) species and the
8 aqueous phase adsorption of Hg(II) to PM. Fig. 1 depicts the mercury reaction
9 pathways both in the gas and aqueous phase while the detailed reactions and their rate
10 constants are summarized in Table 1. In line with most global mercury models,
11 GNAQPMS-Hg does not include dynamic air-surface exchange during Mercury
12 Depletion Events (MDEs) in Polar regions (Schroeder et al., 1998) due to lack of
13 fundamental data.

14 In the gas phase, Hg(0) is oxidized to Hg(II) by O₃, OH, hydrogen peroxide (H₂O₂),
15 hydrogen chloride (HCl) and molecular chlorine (Cl₂). The oxidized products of these
16 five reactions are assumed to be in the gas phase. According to Lin et al. (2004), OH
17 and O₃ are the dominant oxidants in the continental troposphere while Cl and Br
18 dominate Hg(0) oxidation in the marine boundary layer and the upper troposphere. In
19 the aqueous phase, Hg(0) is oxidized to Hg(II) by dissolved O₃, OH, and Cl₂, and
20 Hg(II) can be reduced back to Hg(0) via reaction with HO₂ and by the formation of
21 sulfite complexes. In addition, adsorption of Hg(II) species on atmospheric particulate
22 matter (PM) is simulated using an adsorption coefficient ($K = 34 \text{ L g}^{-1}$) recommended
23 by Seigneur et al. (1998).

24 As shown in Table 1, the mercury chemistry requires the concentrations of several
25 non-mercury species, among which O₃, OH, HO₂, H₂O₂, SO₂, HCl and PM are
26 simulated online with GNAQPMS-Hg. However, Cl₂ is not explicitly simulated, and a
27 typical vertical profile of Cl₂ concentrations is therefore prescribed. The Cl₂
28 concentrations are specified to be 100 ppt at the surface, 50 ppt aloft at night, 10 ppt
29 during daytime over the oceans, and zero over land (Seigneur et al., 2001).

1 **2.2.2 Bromine oxidation**

2 In order to test the effect of bromine (Br) oxidation reactions on global Hg
3 concentrations, five Br chemical reactions in the gas phase are added in addition to
4 the O₃-OH oxidation mechanism. The detailed description of the Br chemical
5 reactions and their implementation in the model is shown in Section S1.1 in the
6 supplement. A model sensitivity experiment with additional Br oxidation reactions
7 was conducted and compared to the base case simulation with O₃-OH oxidation
8 mechanism. Fig. S1 in the supplement shows the difference of surface TGM
9 concentrations resulting from introducing Br oxidation reactions. Decrease in TGM
10 concentrations is found in the whole globe. This is because additional Br chemistry
11 transforms more Hg(0) into Hg(II), which subsequently enhances the deposition of
12 Hg(II), leading to the reduction of TGM concentrations. Larger TGM reduction is
13 found in the Northern Hemisphere than in the Southern Hemisphere. In general, the
14 change in TGM concentration is less than 0.2 ng m⁻³ in most areas which indicates
15 that introducing Br chemistry seems to have little impact on overall TGM
16 magnitudes and patterns. These results are similar to Lei et al. (2013) which test the
17 impact of Br chemistry using the CAM-Chem-Hg model. Although adding the Br
18 chemistry does not significantly change the TGM pattern, but it may affect the
19 gaseous Hg partitioning between Hg(0) and Hg(II), and hence may affect the global
20 Hg deposition patterns. More in-depth tests and analysis are needed to address these
21 impacts in the future. In the following sections, we still use the base case simulated
22 results without considering the possible effects of Br chemistry.

23 **2.2.3 Gas-particle partitioning of Hg(II)**

24 Recent studies suggested that gas-particle partitioning of Hg(II) is an important
25 process affected global Hg concentrations and deposition (Amos et al., 2012). To test
26 these effects, an empirical mechanism of gas-particle partitioning of Hg(II) was added
27 to the GNAQPMS-Hg model. The detailed description of this mechanism and its
28 implementation in the model is shown in Section S1.2 in the supplement. A model

1 sensitivity experiment with Hg(II) gas-particle partitioning module was conducted and
2 compared to the base case simulation with all Hg(II) existing in the gas phase. Figs.
3 S2-3 in the supplement show the change fraction of surface TGM concentrations and
4 oxidized Hg concentrations resulting from introducing the Hg(II) gas-particle
5 partitioning mechanism. As expected, TGM concentrations decrease while oxidized
6 Hg concentrations increase in the whole globe. The change fractions of TGM and
7 oxidized Hg concentrations are smaller than 0.1 over the middle latitude of the
8 Northern Hemisphere, and even smaller than 0.05 over China. Considering that the
9 base case simulation has overestimated oxidized Hg concentrations in most areas,
10 introducing the mechanism of gas-particle partitioning of Hg(II) would further
11 increase this model discrepancy. Therefore, we still use the base case simulated
12 results without considering the possible effects of gas-particle partitioning of Hg(II) in
13 the following sections.

14 **2.3 Mercury deposition**

15 Deposition is the leading removal process of atmospheric mercury, and also a major
16 cause of mercury contamination in soil and water. Studies have shown that both dry
17 and wet removal pathways are equally significant for the total deposition of mercury
18 (Pirrone and Keating, 2010; Lin et al., 2006).

19 Dry deposition of Hg(0), Hg(II) and Hg(P) is accounted for in the GNAQPMS-Hg
20 model, and simulated with the Wesely (1989) resistance model, which considers the
21 effect of different land cover types and characterizes the diurnal variation of dry
22 deposition velocities. The Henry's Law constant for Hg(0) is set to be 0.11 M atm^{-1}
23 (Lin and Pehkonen, 1999) with a temperature factor of -4970 K (Clever et al., 1985),
24 and the surface reactivity is set to zero. Hg(II) represents HgCl_2 and Hg(OH)_2 . Its
25 Henry's Law constant is assumed to be the same as HNO_3 because they have similar
26 solubility (Bullock and Brehme, 2002). Like HNO_3 , Hg(II) has a strong tendency to
27 stick to surfaces and its dry deposition occurs readily, so the surface resistance for
28 Hg(II) in the dry deposition scheme is set to zero. The Hg(P) dry deposition velocity
29 is set equal to that for sulfate, similar to that applied in the CMAQ-Hg and

1 STEM-Hg model (Bullock and Brehme, 2002; Pan et al., 2008). More detailed
2 description of the dry deposition scheme used in the model is given in Section S2.1
3 in the supplement. Model intercomparison studies demonstrate that there are still
4 very large uncertainties in Hg dry deposition estimates (Bullock et al., 2008), and
5 this can be ascribed to the wide range of treatments and physical parameters for dry
6 deposition used in different models.

7 The wet deposition of Hg includes in-cloud and below-cloud scavenging. In-cloud
8 scavenging is dependent on cloud and rain water content, species solubility and
9 chemical transformation in the liquid phase, while below-cloud scavenging depends
10 mainly on total rainfall intensity and washout efficiency. Among the three forms of
11 mercury, wet deposition of Hg(0) is minor compared to Hg(II) and Hg(P) due to its
12 low solubility. Therefore, Hg(0) oxidation will enhance total Hg wet deposition. In
13 the GNAQPMS-Hg model, wet deposition of Hg species is calculated through
14 adapting the RADM mechanism. The physical properties (e.g. Henry's Law constant,
15 surface reactivity, molecular diffusivity) used are the same as those in the dry
16 deposition module. More detailed description of the wet deposition scheme used in
17 the model is given in Section S2.2 in the supplement. Currently, the uncertainties of
18 Hg wet deposition simulation are mainly from the assumptions made in the cloud
19 scavenging process and the uncertainty associated with the precipitation fields
20 (Seigneur et al., 2001; Lin et al., 2006).

21 **2.4 Mercury emissions**

22 We include anthropogenic emissions, biomass burning emissions, geogenic
23 emissions, land reemission and ocean emissions (including reemission) of Hg in the
24 model. Emissions from artisanal mining and volcanoes are neglected due to lack of
25 fundamental data. The former is estimated to be 400 Mg yr⁻¹, and the latter 90 Mg
26 yr⁻¹, and they account for about 5% and 1% of global total Hg emissions (Pirrone et
27 al., 2010). Note that biomass burning emissions, geogenic emissions, land and ocean
28 emissions are all treated as Hg(0). Global Hg emissions in the model are compared
29 to previous studies in Table 2, and their spatial distributions are given in Figs. S4-S6

1 in the supplement.

2 Anthropogenic emissions in 2000 are derived from the Arctic Monitoring and
3 Assessment Programme (AMAP) inventory (Pacyna et al., 2006; Wilson et al.,
4 2006). This inventory has a horizontal resolution of $0.5^{\circ} \times 0.5^{\circ}$ and no seasonal
5 variation. Following Selin et al. (2008), we increase the Asian ($0^{\circ} \sim 60^{\circ} \text{N}$, $65^{\circ} \sim 150^{\circ} \text{E}$)
6 Hg(0) emissions in the AMAP inventory by 50% (about 300 Mg yr^{-1}) to account for
7 the regional underestimation identified by Jaffe et al. (2005). The modified inventory
8 has a total emission of 2488 Mg yr^{-1} , with Hg(0), Hg(II) and Hg(P) accounting for
9 63%, 29% and 8% respectively. The major source regions are Asia and Africa,
10 accounting for 59% (1480 Mg yr^{-1}) and 16% (399 Mg yr^{-1}), while Europe and North
11 America contribute only 7% and 6%. China has the largest emissions at country
12 level (about 785 Mg yr^{-1}), contributing 53% and 32% to the Asian and global
13 anthropogenic Hg emissions, respectively. It is noted that the emissions over South
14 Africa in this inventory were reported to be flawed (AMAP/UNEP, 2008) and much
15 higher than reality. The effects of these flawed emissions on the simulated results
16 were assessed in Section S3 in the supplement.

17 Biomass burning emissions are specified by mapping an annual mean value of 675
18 Mg yr^{-1} (Friedli et al., 2009) to the spatial and temporal distribution of CO biomass
19 burning emissions from the IPCC-AR5 (Intergovernmental Panel on Climate Change
20 Fifth Assessment Report) emissions inventory (Lamarque et al., 2010). The regional
21 and monthly emission amounts are prescribed based on Friedli et al. (2009). A
22 similar method has been used by Jung et al. (2009).

23 The geogenic emissions here represent mobilization of Hg by degassing from
24 geological reservoirs. Following Selin et al. (2007), we consider a geogenic source
25 of 500 Mg yr^{-1} distributed according to the locations of Hg mines (Frank, 1999) as an
26 indicator of Hg deposits. No temporal variation is applied to the geogenic emissions.

27 Land and ocean emissions are not dynamically calculated in the model due to the
28 large uncertainties associated with current parameterizations. Consistent with several
29 previous studies (Selin et al., 2007; Seigneur et al., 2001), the global annual land
30 reemission of Hg is assumed to be 1500 Mg yr^{-1} . The biogenic CO emissions from

1 the Global Emission Initiative (GEIA) inventory (Guenther et al., 2006) are used as
2 spatial and temporal surrogates to map the land reemission. Regional emission totals
3 from different latitude zones and land uses are prescribed based on Mason (2009).

4 Ocean emissions in our model are specified as 5000 Mg yr⁻¹ (including
5 reemission), close to the estimates of Selin et al. (2008). Similarly, ocean emissions
6 are mapped according to the distribution of ocean biogenic CO emissions from the
7 Precursors of Ozone and their Effects in the Troposphere (POET) inventory (Granier
8 et al., 2005). Additionally, ocean emissions are adjusted to reflect several
9 distribution characteristics: 1) ocean emissions are high in summer but low in winter
10 (Strode et al., 2007), 2) ocean emissions are largest in the Tropics and downwind of
11 industrial regions (Strode et al., 2007; Soerensen et al., 2010b), and 3) ocean
12 emissions are large at mid and high latitudes in the Southern Hemisphere due to high
13 wind speeds (Selin et al., 2008).

14 **2.5 Model setup**

15 Two nested domains covering the whole globe and East Asia are configured in this
16 study. The horizontal resolutions are 1°x1° and 0.33°x0.33°, respectively. Vertically,
17 the model uses 20 terrain-following layers from the surface to 20 km a.s.l., with a
18 decreasing resolution with height. Roughly, the lowest 14-18 layers are in the
19 troposphere and the remaining layers are in the stratosphere. The time step in the
20 model calculation is 600 s. The input/output frequency is 6h in the global domain but
21 3h in the nested domain. The meteorological fields are provided by the global
22 version of the Weather Research and Forecasting (WRF) model. The atmospheric
23 lifetime of Hg(0) is 0.5-2 year (Schroeder and Munthe, 1998), and so to ensure
24 mixing through the global troposphere and approach steady-state, we conduct the
25 simulation for a 4-year period, with the first 3 years used for initialization and the
26 last year (2001) used for analyses.

27 Emissions of reactive gases and aerosols used in this study are from several
28 databases: 1) the IPCC-AR5 anthropogenic and biomass burning emissions for 2000
29 (Lamarque et al., 2010); 2) the GEIA biogenic emissions for 2000 (Guenther et al.,

1 2006) and lightning emissions of nitric oxide (NO_x) for 1983–1990 (Price et al.,
2 1997); 3) the POET ocean emissions of volatile organic compounds (VOCs) for
3 2000 (Granier et al., 2005); 4) the soil NO_x emissions for 2001 from Yan et al. (2005).
4 All emissions are interpolated and remapped to match the model grids of the global
5 and nested domains. The initial and top boundary conditions for O₃, NO_x, and CO
6 are taken from a global chemical transport model (MOZART-V2.4) with 2.8°
7 resolution (Horowitz et al., 2003).

8 Two model simulations, with and without Chinese primary anthropogenic Hg
9 emissions, are carried out in this study. The differences between the two simulations
10 are attributed to the influence of Chinese primary anthropogenic Hg emissions.

11 **3 Model evaluation**

12 **3.1 Observational data**

13 Compared to reactive gases and aerosols, atmospheric Hg measurements are still
14 quite sparse. Routine monitoring networks for atmospheric Hg concentrations and
15 deposition have only been established in Europe and North America. Lack of Hg
16 observational data is a great restriction against advancing our understanding of
17 global Hg cycling and improving our skill in modeling. There is an urgent need to
18 establish a coordinated global Hg monitoring network for current Hg study
19 (Sprovieri et al., 2010; Keeler et al., 2009).

20 The observational dataset in this study is based partly on the database shared by the
21 GEOS-Chem Hg modeling group (public access at [https://github.com/noelleselin/
22 HgBenchmark](https://github.com/noelleselin/HgBenchmark); Selin et al., 2007; Selin et al., 2008; Holmes et al., 2010). This is
23 supplemented with scattered Hg observations across East Asia collected from the
24 literature. The observations used in this study are summarized as follows: 1)
25 long-term TGM/GEM (gaseous elemental mercury) measurements at 51 land sites,
26 with 49 in the Northern Hemisphere and 2 in the Southern Hemisphere; 2) long-term
27 RGM/TPM measurements at 26 land sites, all in the Northern Hemisphere; 3)
28 short-term Hg species measurements from 6 ship cruises; 4) wet deposition

1 measurements from the MDN (the Mercury Deposition Network in North America,
2 <http://nadp.sws.uiuc.edu/nadpdata/mdnalldata.asp>) and EMEP (the European
3 Monitoring and Evaluation Programme,
4 <http://www.nilu.no/projects/ccc/emepdata.html>) monitoring networks, with 51 and 8
5 sites respectively; 5) dry and wet deposition measurements at 19 sites in East Asia.
6 Further information about the measurement sites and data sources is given in Tables
7 S2-S5 in the supplement. It should be noted that the time periods of the measurements
8 do not all match with those of the simulation, and this difference may partially explain
9 any model–observation discrepancies. The influence of the mismatch of time periods
10 when comparing the simulated results with the observations was qualitatively
11 analyzed and shown in Section S4.1 in the supplement.

12 **3.2 Global mercury budget**

13 Fig. 2 gives the global mercury budget in GNAQPMS-Hg, including the cycling
14 among atmosphere, ocean and land. The total atmospheric burden of Hg is 5546 Mg,
15 with Hg(0), Hg(II), and Hg(P) contributing 90%, 9% and 1%, respectively. Therefore,
16 mercury in the atmosphere exists mainly as Hg(0). Total emissions and deposition of
17 Hg are 5163 Mg yr⁻¹ and 2866 Mg yr⁻¹ over land (a net source), and are 5000 Mg yr⁻¹
18 and 7297 Mg yr⁻¹ over ocean (a net sink), indicating that Hg is transported from land
19 to ocean. For total deposition of Hg species, Hg(0) and Hg(II)/Hg(P) account for 38%
20 and 62% over the earth's surface. Over land, deposition of Hg(II)/Hg(P) is more
21 prominent than that of Hg(0), while they are both important over the ocean. Our
22 results for total Hg deposition over ocean and Hg(II)/Hg(P) deposition over land are
23 very close to that of GEOS-Chem (Selin et al., 2008). However, Hg(0) deposition
24 over land derived from GNAQPMS-Hg is much smaller. This may be due to the
25 lower reactivity coefficient used in the dry deposition module in GNAQPMS-Hg
26 (zero in GNAQPMS-Hg but 10⁻⁵ in GEOS-Chem), which produces a lower dry
27 deposition velocity for Hg(0).

28 Table 2 compares the GNAQPMS-Hg TGM budget and lifetime to those from
29 previous modeling studies. The TGM sources, sinks, burden and lifetime estimated

1 from GNAQPMS-Hg are all in the range determined by previous studies. Taking the
2 TGM lifetime as an example, the reported range is 0.5-1.7 years and it is 0.54 years
3 for GNAPQMS-Hg. In addition, similar to the results of GEOS-Chem (Selin et al.,
4 2007) and CAM-Chem-Hg (Lei et al., 2013), Hg dry deposition in GNAQPMS-Hg
5 dominates globally over wet deposition. Dry and wet deposition account for 78%
6 and 22%, respectively.

7 **3.3 Total gaseous mercury (TGM)**

8 As shown in Fig. 3, the main characteristics of the spatial distribution of TGM are
9 captured well by the model. High surface TGM concentrations are found in or
10 downwind of areas with intensive mercury-relative mining (e.g. Western USA) and
11 rapid industrialization (e.g. East Asia). In particular, TGM concentrations even
12 exceed 3 ng m^{-3} in eastern China. Both model simulation and observations show a
13 significant surface interhemispheric gradient in TGM (Fig. 3 and Fig. 4). Based on
14 background observations, Lindberg et al. (2007) reported that mean Hg(0)
15 concentrations were $1.5\text{--}1.7 \text{ ng m}^{-3}$ in the Northern Hemisphere and $1.1\text{--}1.7 \text{ ng m}^{-3}$
16 in the Southern Hemisphere. Lamborg et al. (2002) also estimated the range of
17 north-south interhemispheric TGM concentration ratios for surface air as 1.2–1.8.
18 Our model results share a general similarity with these studies. In GNAQPMS-Hg,
19 surface mean TGM concentrations in the Northern and Southern Hemisphere are
20 1.56 and 1.23 ng m^{-3} , and the derived interhemispheric ratio is 1.27. However, it
21 should be noted that GNAQPMS-Hg is systematically biased low relative to cruise
22 observations in the Northern Hemisphere, which leads to underestimation of the
23 TGM interhemispheric ratio compared with the range (1.49 ± 0.12) reported by
24 Temme et al. (2003) based on observations from several Atlantic cruises. This
25 disagreement was also found by several previous modeling studies (Seigneur et al.,
26 2004; Selin et al., 2007), and can be attribute to the inability of current models to
27 reproduce the air-sea exchange of Hg reasonably (Soerensen et al., 2010a). More
28 specifically, this discrepancy is due to upwelling mercury from the sub-surface
29 ocean, possibly reflecting the legacy of past anthropogenic emissions (Holmes et al.,

1 2010), and has been partially demonstrated by Soerensen et al. (2012). In general,
2 the simulated TGM concentrations match observations within a factor of two (Fig.
3 10). The correlation coefficient (R) and normalized mean bias (NMB) between
4 model results and observations from 51 land sites are 0.7 and -18%, respectively
5 (Table 3).

6 Fig. 5 illustrates the mean seasonal variations of surface TGM concentrations in
7 North America, Europe, East Asia, the Arctic, the Antarctic (Neumayer) and South
8 Africa (Cape Point). In northern mid-latitudes, TGM concentrations are high in
9 winter but low in summer. This seasonality can be reproduced well by
10 GNAQPMS-Hg. The summer low is caused by high OH concentrations and frequent
11 precipitation (Bergan and Rodhe, 2001). Compared with observations, the simulated
12 TGM monthly variations are stronger in North America but weaker in East Asia. The
13 site by site comparisons in East Asia are shown in Fig. S9 in the supplement. We can
14 see that nested simulation can well improve model performance in simulated TGM
15 monthly variation in East Asia. At Arctic and Antarctic sites, TGM shows a spring
16 minimum driven by MDEs and a summer maximum driven by reemission from the
17 snowpack (Steffen et al., 2005). The summer maximum is captured by
18 GNAQPMS-Hg because high reemission in polar summer has been taken into
19 account in our land reemission inventories. However, due to missing halogen
20 chemistry, the model fails to reproduce the spring minimum. At Cape Point, both
21 observed and simulated TGM show little seasonal variation. However, simulated
22 monthly TGM concentrations are systematically biased high (NMB is 87%), which
23 can be attributed to the flawed anthropogenic emissions in the AMAP emission
24 inventories over South Africa (AMAP/UNEP, 2008). By updating the anthropogenic
25 emissions over South Africa, the simulated TGM concentrations at Cape Point
26 decrease from 1.77 ng m^{-3} to 1.23 ng m^{-3} , more close to the observed values (See
27 Section S3 in the supplement).

28 Additional evaluation and analyses of simulated diurnal and vertical variation of
29 TGM concentrations are given in Section S4.2 in the supplement.

1 **3.4 Oxidized mercury**

2 Fig. 3 also shows the global distribution of oxidized mercury (defined as the sum of
3 RGM+TPM in the observations and Hg(II)+Hg(P) in the model). Similar to TGM, a
4 pronounced north-south interhemispheric gradient is found for surface
5 concentrations of oxidized mercury, which is consistent with the global distribution
6 of emissions. Both model simulation and observations indicate that oxidized
7 mercury concentrations are much higher in East Asia than North America and
8 Europe. Compared to scarce available observations, oxidized mercury concentrations
9 are overestimated by GNAQPMS-Hg in most parts of the world (except East Asia).
10 This discrepancy may partially be attributed to excessive oxidation of Hg(0) by
11 relatively high concentrations of OH and O₃ (especially over the ocean) and
12 uncertainties concerning Hg chemical speciation in emission inventories. The
13 simulated tropospheric mean OH concentration is 1.41×10^6 molec cm⁻³. This is at the
14 high end of the concentration range ($0.65\text{--}1.56 \times 10^6$ molec cm⁻³) summarized by
15 Lawrence et al. (2001) and is about 27% higher than the ensemble mean
16 ($11.1 \pm 1.8 \times 10^5$ molec cm⁻³) of the Atmospheric Chemistry and Climate Model
17 Intercomparison Project (ACCMIP) models (Voulgarakis et al., 2013). The simulated
18 mean surface O₃ in the North Pacific and North Atlantic is overestimated by 27%
19 and 34% compared to observations from the WDCGG (World Data Centre for
20 Greenhouse Gases) network, although concentrations over land are reproduced
21 relatively well (see Figs. S10-S11 in the supplement). Besides, uncertainties of Hg
22 chemistry (e.g. gas-particle partitioning of RGM, in-plume reduction of RGM) and
23 deposition processes in the present model might also contribute to this discrepancy.
24 Overall, the simulated oxidized mercury concentrations agree with observations
25 within a factor of five (Fig. 10). The statistical indicators, R and NMB, calculated
26 from 26 land sites are 0.53 and 3% (Table 3), respectively.

27 **3.5 Wet deposition**

28 Wet deposition is mainly determined by the distribution of precipitation and Hg

1 concentrations. Fig. 6 and Fig. 7 evaluate the simulated annual Hg wet deposition
2 and accumulated precipitation over North America, Europe and East Asia. In general,
3 GNAQPMS-Hg reproduces the spatial patterns of Hg wet deposition relatively well.

4 Over North America, the maximum wet deposition occurs in the southeast,
5 corresponding to high OH concentrations and frequent precipitation there, while less
6 wet deposition occurs in the west and north, where there is much less precipitation.
7 GNAQPMS-Hg predicts the magnitude of mean wet deposition within 5% and
8 shows a good spatial correlation ($R=0.76$) (Table 3). These results are similar to
9 those of GEOS-Chem (Selin et al., 2007). However, it should be also noted that
10 precipitation in the southeast is slightly overestimated by the model.

11 Over Europe, model performance for wet deposition and precipitation are better
12 than over North America and East Asia. High spatial correlation between the
13 simulated and observed results are found for both wet deposition ($R=0.78$) and
14 precipitation ($R=0.86$), and the NMBs are both less than 5% (Table 3).

15 Over East Asia, Hg wet deposition is not only related to the precipitation pattern
16 but also the local Hg emissions, especially in the southwest and Jilin province of
17 China, and in Central Japan. Model performance for wet deposition over East Asia is
18 poorer than over Europe and North America. Although the spatial distribution and
19 magnitude of precipitation over East Asia are seemingly well reproduced ($R=0.64$
20 and $NMB=-6\%$), a large underestimation ($NMB=-61\%$) of wet deposition is found
21 here. Specifically, this is because the model fails to capture the high wet deposition
22 at certain sites. For example, the observed wet deposition over Shanghai and
23 Changchun are 251 and $108 \mu\text{g m}^{-2} \text{yr}^{-1}$ while the corresponding simulated values are
24 only 25 and $13 \mu\text{g m}^{-2} \text{yr}^{-1}$. This suggests that it is hard for models with coarse
25 horizontal resolution to characterize the high local mercury pollution in China. The
26 difference between the simulated and observed time periods and uncertainties in the
27 emission inventories may also contribute to these discrepancies.

28 Fig. 8 further compares the simulated seasonal cycle of wet deposition with
29 measurements at MDN sites over North America and EMEP sites over Europe. No
30 monthly wet deposition observations are available over East Asia. Wet deposition

1 and precipitation share similar monthly variations, with high values in summer and
2 autumn and low values in winter, as shown by both observations and simulation. In
3 summer and autumn, the variation in wet deposition and precipitation among sites is
4 larger than for other seasons, and this is evident from the greater variability in Fig. 8.
5 GNAQPMS-Hg tends to overestimate wet deposition and precipitation in July and
6 August over North America.

7 **3.6 Dry deposition**

8 Due to limited observations, only Hg dry deposition over East Asia is evaluated in
9 this study. It should be noted that data (Table S5 in the supplement) used to evaluate
10 model simulation of dry deposition is not directly measured, but is inferred or
11 estimated based on measurements of total Hg in through fall and rainwater, wet
12 deposition and atmospheric concentrations. Associated with local Hg emissions,
13 high dry deposition mainly occurs over central eastern China and central Japan (Fig.
14 9). The modeled dry deposition has a good spatial correlation with observations
15 ($r=0.81$), but there is a substantial negative bias (NMB=-42%, Table 3). In general,
16 the simulated dry deposition agrees with observations within a factor of five (Fig.
17 10). Over Japan, the model results are biased high by a factor of 2-5, which may be
18 caused by overestimation of Hg(II) and Hg(P) emissions and missing model
19 mechanism to deal with fast in-plume reduction of Hg(II) (Vijayaraghavan et al.,
20 2008; Amos et al., 2012; Zhang et al., 2012). Taking Tokyo as an example, observed
21 Hg(P) is only 98 pg m^{-3} while the simulated value is as high as 648 pg m^{-3} . Modeling
22 studies conducted by Pan et al. (2008) using the STEM-Hg model also found large
23 overestimation in dry deposition over Japan. Conversely, the model results are biased
24 low by a factor of 2-5 over China, which indicates probable underestimation of
25 Chinese Hg emissions.

26 **3.7 Model performance summary and comparison**

27 In this section, we summarize the statistical performance of GNAQPMS-Hg for
28 TGM, oxidized mercury, and wet and dry deposition, compare the model

1 performance over East Asia, North America and Europe, and assess the effects of
2 horizontal resolution on model predictions over East Asia. As shown in Fig. 10, the
3 simulated TGM and wet deposition are within a factor of two of the corresponding
4 observations and within a factor of five for oxidized mercury and dry deposition.
5 The statistical performance of GNAQPMS-Hg is comparable with that of other
6 state-of-the-art Hg models (Bullock et al., 2008; Ryaboshapko et al., 2007; Pirrone
7 and Keating, 2010).

8 **3.7.1 East Asia versus North America and Europe**

9 As illustrated in Table 3, the model statistical performance for all Hg parameters in
10 North America and Europe is better than in East Asia. For example, the RMSEs
11 between simulated and observed TGM over North America and Europe are 0.58 and
12 0.17 ng m⁻³ but up to 3.61 ng m⁻³ over East Asia. The poor model performance over
13 East Asia is probably caused by the following reasons. Firstly, there are differences
14 between simulated and observed data periods. Hg measurements over East Asia
15 (especially China) are mainly taken from recent years, and the observed values are
16 higher than in year 2001, which may lead to model underestimation. Hg
17 anthropogenic emissions in China had increased by 164% during 1992-2007 (Liang
18 et al., 2013) is an evidence. Secondly, there is a much higher spatial variation ratio
19 (SVR, see Table 3) for Hg parameters in East Asia than North America and Europe.
20 This implies that there are very intense spatial variations in surface Hg
21 concentrations and deposition over East Asia which cannot be resolved at the coarse
22 horizontal resolution used in global models (see Section 3.7.2). Thirdly, there are
23 large uncertainties in emission inventories over East Asia. Large underestimations in
24 Hg anthropogenic emissions over East Asia have been demonstrated in several
25 previous studies (Jaffe et al., 2005; Pan et al., 2007; Friedli et al., 2004; Song et al.,
26 2015). This is consistent with the simulated results in this study. Except the above
27 factors, missing of some chemical and physical processes (e.g. gas-particle
28 partitioning of Hg(II), in-plume reduction of Hg(II), dynamic land reemission) in the
29 present model might also contribute to the poor model performance over East Asia.

1 3.7.2 Global versus nested simulations

2 In order to assess the impact of resolution on model predictions, an online nested
3 simulation with higher resolution ($0.33^\circ \times 0.33^\circ$) over East Asia was conducted and
4 compared to the global simulation with lower resolution ($1^\circ \times 1^\circ$). Emissions,
5 meteorology, deposition and chemistry are self-consistent between the global and
6 nested domains. The nested simulation uses higher resolution model inputs (e.g.
7 topography, meteorology, emissions) and thus has the potential to better resolve high
8 spatial variability of Hg concentrations and deposition in regional and local scales.

9 Fig. 7 and Fig. 9 compare the spatial distributions of simulated annual mercury
10 wet deposition, accumulated precipitation and dry deposition over East Asia between
11 the global and nested simulations. Although the global and nested simulations
12 predict similar large scale patterns for Hg deposition, the nested simulation resolves
13 many fine features which are lost in the global simulation by horizontal averaging.
14 Firstly, in the nested domain, high deposition fluxes become more concentrated in
15 regions with large emissions or precipitation resulting in higher spatial variability in
16 deposition. Secondly, the nested simulation reveals elevated wet deposition in
17 southwest China due to frequent orographic and convective precipitation. Finally, the
18 nested simulation shows a more detailed land/ocean contrast in deposition over
19 coastal regions. For example, over the coastal regions of southeast China and Japan,
20 wet deposition increases due to scavenging of local emissions and enhanced
21 precipitation (Fig. 7) while dry deposition decreases associated with the lower dry
22 deposition velocity of Hg(0) over land than over ocean (Fig. 9). Our results are
23 similar to those of Zhang et al. (2012) who conducted a nested simulation of Hg over
24 North America using the GEOS-Chem model. More comparisons about the
25 differences of dry and wet deposition and Hg budgets over East Asia between the
26 two simulations are given in Fig. S16 and Table S6 in the supplement.

27 Fig. 11 and Table 3 further quantitatively compare the model performance over
28 East Asia between the global and nested domains. In the Taylor diagram (Taylor,
29 2001), the position of each circle (or square) quantifies how closely the simulated

1 results match observations. We can see that the simulated precipitation, oxidized Hg,
2 wet and dry deposition agree better with observations in the nested domain than in
3 the global domain (Fig. 11). The largest improvement is found in the simulated wet
4 deposition. Specifically, the statistical parameter R for simulated wet deposition
5 increases from 0.36 to 0.78, the NMB decreases from -61% to -28%, and the RMSE
6 decreases by 24% (from 60.1 to 45.5 $\mu\text{g m}^{-2} \text{yr}^{-1}$) (Table 3). But for TGM, oxidized
7 Hg and dry deposition, the statistical parameters do not change significantly. For
8 example, the RMSEs of simulated oxidized Hg and dry deposition decrease by 7%
9 and 2% respectively, but increase by 7% for simulated TGM.

10 **3.7.3 Online versus offline nested simulations**

11 In order to further justify the online nested method, several model sensitivity
12 experiments were conducted and the simulated results were compared to
13 observations over East Asia. In the base simulation, the online nested method was
14 used and the nested domain get boundary conditions from the global domain every
15 10 minutes. In the sensitivity simulations, the offline method was used and the
16 boundary conditions were applied at 3 or 6 hours. The differences between the base
17 and the sensitivity simulations were mainly caused by different frequency of
18 boundary conditions. As shown in Table 4, the model performances are similar
19 between the two sensitivity simulations (with 3 and 6 hour offline boundary
20 conditions respectively). While the model performances in the base simulation are
21 slightly better than those in the sensitivity simulations. The largest improvement is
22 found in the simulated oxidized mercury. Specifically, the statistical parameter R for
23 simulated oxidized mercury increases from 0.41 to 0.45, the NMB decreases from
24 -18% to -12%, and the RMSE decreases by 4% compared to the simulated results
25 with 6 hour offline boundary conditions. For wet deposition, little changes are found.
26 This is because Hg wet deposition is not only affected by air concentrations but also
27 precipitation. These results confirmed the effectiveness of the online nested method.

1 **4 Impacts of Chinese primary anthropogenic sources on global Hg** 2 **levels**

3 Fig. 12 shows the contribution of Chinese primary anthropogenic sources (not
4 including reemission) to annual mercury surface concentrations and total deposition
5 in the Northern Hemisphere, and Fig. 13 gives the corresponding mean percentage
6 contributions over different world regions (defined in Fig. S17 in the supplement), as
7 derived from a sensitivity simulation with Chinese anthropogenic emissions shut off.
8 In general, the largest percentage contribution is found in China itself, followed by
9 neighbouring regions like the Korean Peninsula, Southeast Asia, Mongolia and Japan,
10 but they are relatively small in other regions. Specifically, domestic anthropogenic
11 emissions contribute on average 0.6 ng m^{-3} (ranging from below 0.1 to above 3.0) to
12 surface Hg concentrations and $18.4 \text{ } \mu\text{g m}^{-2} \text{ yr}^{-1}$ (ranging from below 2.0 to above
13 50.0) to total deposition in China. They account for about 30% and 62% on a
14 national basis, respectively. The domestic contribution to deposition consists mainly
15 of the deposition of directly emitted Hg(II) and Hg(P) near sources and deposition of
16 Hg(II) formed by oxidation of Chinese Hg(0). For neighboring regions, the Chinese
17 anthropogenic contributions to surface Hg concentrations and deposition are also
18 large. For example, the percentage contributions are 11% ($0.2\text{-}0.6 \text{ ng m}^{-3}$) and 15.2%
19 ($8\text{-}20 \text{ } \mu\text{g m}^{-2} \text{ yr}^{-1}$) over the Korean Peninsula, 10.4% ($0.1\text{-}0.6 \text{ ng m}^{-3}$) and 8.2% ($1\text{-}12$
20 $\text{ } \mu\text{g m}^{-2} \text{ yr}^{-1}$) over Southeast Asia, and 5.7% ($0.1\text{-}0.4 \text{ ng m}^{-3}$) and 5.9% ($2\text{-}15 \text{ } \mu\text{g m}^{-2}$
21 yr^{-1}) over Japan. For regions far away from China, the percentage contributions are
22 small. They are 4.2% ($0.06\text{-}0.1 \text{ ng m}^{-3}$) and 4.8% ($0.5\text{-}4 \text{ } \mu\text{g m}^{-2} \text{ yr}^{-1}$) over North
23 America, and 3.5% (below 0.08 ng m^{-3}) and 3.0% (below $2.0 \text{ } \mu\text{g m}^{-2} \text{ yr}^{-1}$) over
24 Europe. The percentage contributions over North America determined from our
25 simulation are comparable with the modeling study of Lei et al. (2013). They
26 estimated that around 7% of TGM concentrations and 9% of total Hg deposition in
27 the United States resulted from transpacific transport of Asian anthropogenic
28 emissions. Given that about 53% of Asian anthropogenic Hg emissions are from

1 China, it is reasonable that our estimated contributions are a little smaller than those
2 reported by Lei et al. (2013).

3 Finally, there are another two issues which need to be addressed. Firstly, the above
4 analysis mainly focuses on regional average contributions. However, the percentage
5 contributions vary geographically inside the region. As shown in Fig. 12,
6 contributions of domestic anthropogenic emissions to total deposition in Central
7 Eastern China can exceed $40 \mu\text{g m}^{-2} \text{yr}^{-1}$, but they are below $5 \mu\text{g m}^{-2} \text{yr}^{-1}$ in Western
8 China. Similarly, previous studies have found that Asia emissions make a much
9 larger contribution to Hg deposition in the Western USA than in the Eastern USA
10 (Seigneur et al., 2004; Strode et al., 2008). Secondly, the contributions from
11 reemission of previously deposited anthropogenic Hg (treated as natural land or
12 ocean reemission in GNAQPMS-Hg) are not taken into account in this study. Of the
13 natural emissions, only one-third is considered not to be influenced by anthropogenic
14 activities at all (Jung et al., 2009). In addition, according to the modeling study of
15 Selin et al. (2008), 31% (including 22% primary and 9% recycled) of the deposition
16 over USA is from anthropogenic emissions outside of North America. When
17 considering reemission of previously deposited anthropogenic Hg, this suggests that
18 the foreign anthropogenic contribution would increase by about 42% (from 22% to
19 31%). If we apply the same scaling factor to our attribution results, then the
20 estimated Chinese anthropogenic contributions to Hg deposition over North America
21 would increase from 4.8% to 6.8%. Therefore, it is also important to consider the
22 reemission of previously deposited anthropogenic Hg.

23 **5 Conclusions**

24 A global nested atmospheric mercury transport model including Hg emissions,
25 chemical transformation and deposition is introduced in this study. The treatment of
26 Hg chemistry employs the O_3 -OH oxidation and SO_3^{2-} - HO_2 reduction mechanisms.
27 The gas phase reactions of Hg are added to the CBM-Z mechanism, while the
28 aqueous phase reactions and wet deposition of Hg are calculated through adapting

1 the RADM mechanism. The Wesely (1989) resistance model is used to deal with Hg
2 dry deposition. The same meteorological fields, emissions, chemical and physical
3 parameterizations are used in the global and nested domains.

4 The GNAQPMS-Hg model has a global mercury source of 10163 Mg yr⁻¹,
5 including 2488 Mg yr⁻¹ primary anthropogenic emissions, 675 Mg yr⁻¹ biomass
6 burning emissions, 2000 Mg yr⁻¹ land emissions (of which 75% is reemission), and
7 5000 Mg yr⁻¹ from the ocean. Dynamic bidirectional air-surface exchange of Hg is
8 not included in the model. Instead, we simply apply static net emission fluxes to
9 account for natural sources (including reemission) of Hg, with total emission
10 amounts determined based on published estimates.

11 Based on existing routine monitoring networks (e.g. MDN, EMEP) and the
12 published literature, global observations including surface Hg concentrations and
13 deposition are collected for model evaluation. Compared with previous studies,
14 many more observations over East Asia (especially China) are included in our
15 dataset. Model evaluation shows that the spatial distribution and seasonal cycle of
16 Hg concentrations and deposition can be reproduced reasonably well by
17 GNAQPMS-Hg. Overall, the simulated annual TGM and wet deposition match
18 observations within a factor of two, and within a factor of five for oxidized mercury
19 and dry deposition. This performance is comparable with other state-of-the-art Hg
20 models. Some model deficiencies have also been identified. GNAQPMS-Hg is
21 systematically biased low relative to cruise observations in the Northern Hemisphere,
22 due to poor representation of the air-sea exchange mechanism for Hg.
23 GNAQPMS-Hg overestimates oxidized mercury concentrations in most parts of the
24 world which may partially be caused by excessive oxidation of Hg(0) by relatively
25 high concentrations of OH and O₃ and uncertainties associated with Hg chemical
26 speciation in emission inventories. The model performs significantly better in North
27 America and Europe than in East Asia. This can probably be attributed to the large
28 uncertainties in emission inventories, coarse model resolution and inconsistency
29 between the simulation and observation periods in East Asia. An online nested
30 simulation with higher resolution (0.33°x0.33°) over East Asia was conducted to

1 examine the impact of horizontal resolution on model predictions. Relative to the
2 global simulation, the nested simulation can better resolve high spatial variability of
3 Hg concentrations and deposition over East Asia, can better capture features such as
4 higher wet deposition due to orographic and convective precipitation, and land/ocean
5 contrast. Statistically, the RMSE of simulated wet deposition over East Asia is
6 reduced by 24% in the nested simulation.

7 To quantify the impacts of Chinese anthropogenic sources on global Hg levels, a
8 model sensitivity simulation was conducted with Chinese anthropogenic emissions
9 shut off. The results show that these sources contribute 30% and 62% of surface
10 mercury concentrations and deposition over China. Outside of China, the largest
11 percentage contributions of 11% and 15.2% are found in the Korean Peninsula,
12 following by Southeast Asia (10.4% and 8.2%), Mongolia (6.1% and 8.6%), and
13 Japan (5.7% and 5.9%). For regions far away from China, the percentage
14 contributions are relatively small (e.g. 4.2% and 4.8% over North America; 3.5% and
15 3.0% over Europe).

16 To perfect the model, future improvements will be focused on the following
17 aspects: 1) employing dynamic parameterizations for bidirectional air-surface (sea
18 and land) exchange of Hg (Selin et al., 2008; Bash, 2010; Strode et al., 2007) to
19 better reflect natural emissions (including reemission), 2) including fast in-plume
20 reduction of Hg(II) to better characterize Hg(II) distribution near large point sources
21 (Amos et al., 2012), and 3) reducing uncertainties in the anthropogenic Hg emission
22 inventory, especially the Hg speciation profile. Finally, establishment of routine Hg
23 monitoring networks would be also very helpful for enhancing and improving
24 modeling studies in East Asia.

25 **Code availability**

26 Please contact Huansheng Chen (E-mail: chenhuansheng@mail.iap.ac.cn) to obtain the
27 source code of GNAQPMS-Hg.

1 **Acknowledgments**

2 This work is funded by the National Natural Science Foundation of China
3 (41405119), the National Key Technology R&D Program (2014BAC21B02), the
4 Environmental Public Welfare Research Project (201509014), the National Basic
5 Research Program of China (2010CB951800) and the CAS Strategic Priority
6 Research Program (XDB05030200 and XDB05030101). We thank the GEOS-Chem
7 Hg modeling group for sharing observational data of Hg.

8 **References**

- 9 AMAP/UNEP: Technical Background Report to the Global Atmospheric Mercury Assessment,
10 Tech. rep., Arctic Monitoring and Assessment Programme / UNEP Chemicals Branch, <http://www.unep.org/hazardoussubstances/>, 2008.
11
12 AMAP/UNEP: Technical Background Report for the Global Mercury Assessment 2013, Tech.
13 rep., Arctic Monitoring and Assessment Programme AMAP and United Nations Environment
14 Programme (UNEP) Chemicals Branch, [http://www.unep.org/hazardoussubstances/
15 Mercury/Informationmaterials/ReportsandPublications/tabid/3593/Default.aspx](http://www.unep.org/hazardoussubstances/Mercury/Informationmaterials/ReportsandPublications/tabid/3593/Default.aspx), 2013.
16 Amos, H. M., Jacob, D. J., Holmes, C. D., Fisher, J. A., Wang, Q., Yantosca, R. M., Corbitt, E. S.,
17 Galarneau, E., Rutter, A. P., Gustin, M. S., Steffen, A., Schauer, J. J., Graydon, J. A., Louis, V.
18 L. St., Talbot, R. W., Edgerton, E. S., Zhang, Y., and Sunderland, E. M.: Gas-particle
19 partitioning of atmospheric Hg(II) and its effect on global mercury deposition, *Atmos. Chem.*
20 *Phys.*, 12, 591-603, doi:10.5194/acp-12-591-2012, 2012.
21 Ariya, P. A., Khalizov, A., and Gidas, A.: Reactions of gaseous mercury with atomic and
22 molecular halogens: Kinetics, product studies, and atmospheric implications, *J. Phys. Chem. A*,
23 106, 7310-7320, doi:10.1021/jp020719o, 2002.
24 Bash, J. O.: Description and initial simulation of a dynamic bidirectional air-surface exchange
25 model for mercury in Community Multiscale Air Quality (CMAQ) model, *J. Geophys.*
26 *Res.-Atmos.*, 115, D06305, doi:10.1029/2009jd012834, 2010.
27 Bergan, T., and Rodhe, H.: Oxidation of elemental mercury in the atmosphere: constraints
28 imposed by global scale modelling, *J. Atmos. Chem.*, 40, 191-212,
29 doi:10.1023/a:1011929927896, 2001.
30 Bullock, O. R., and Brehme, K. A.: Atmospheric mercury simulation using the CMAQ model:
31 formulation description and analysis of wet deposition results, *Atmos. Environ.*, 36,
32 2135-2146, doi:10.1016/s1352-2310(02)00220-0, 2002.
33 Bullock, O. R., Jr., Atkinson, D., Braverman, T., Civerolo, K., Dastoor, A., Davignon, D., Ku,
34 J.-Y., Lohman, K., Myers, T. C., Park, R. J., Seigneur, C., Selin, N. E., Sistla, G., and
35 Vijayaraghavan, K.: The North American Mercury Model Intercomparison Study (NAMMIS):
36 Study description and model-to-model comparisons, *J. Geophys. Res.-Atmos.*, 113, D17310,
37 doi:10.1029/2008jd009803, 2008.

1 Chang, J. S., Brost, R. A., Isaksen, I. S. A., Madronich, S., Middleton, P., Stockwell, W. R., and
2 Walcek, C. J.: A three-dimensional Eulerian acid deposition model: Physical concepts and
3 formulation, *J. Geophys. Res.-Atmos.*, 92, 14681-14700, doi:10.1029/JD092iD12p14681,
4 1987.

5 Christensen, J. H., Brandt, J., Frohn, L. M., and Skov, H.: Modelling of mercury in the Arctic
6 with the Danish Eulerian Hemispheric Model, *Atmos. Chem. Phys.*, 4, 2251-2257, 2004.

7 Clever, H. L., Johnson, S. A., and Derrick, M. E.: The solubility of mercury and some sparingly
8 soluble mercury salts in water and aqueous-electrolyte solutions, *J. Phys. Chem. Ref. Data*, 14,
9 631-681, 1985.

10 Corbitt, E. S., Jacob, D. J., Holmes, C. D., Streets, D. G., and Sunderland, E. M.: Global
11 source-receptor relationships for mercury deposition under present-day and 2050 emissions
12 scenarios, *Environ. Sci. Technol.*, 45, 10477-10484, doi:10.1021/es202496y, 2011.

13 Dastoor, A. P., and Durnford, D. A.: Arctic Ocean: Is It a Sink or a Source of Atmospheric
14 Mercury, *Environ. Sci. Tehnol.*, 48(3), 1707-1717, 2014.

15 De Simone, F., Gencarelli, C. N., Hedgecok, I. M., Pirrone, N.: Global atmospheric cycle of
16 mercury: a model study on the impact of oxidation mechanisms, *Environ. Sci. Pollut. Res.*, 21,
17 4110-4123, 2014.

18 ENVIRON: User's guide for Comprehensive Air Quality Model with Extensions Version 5.40,
19 ENVIRON International Corporation, Novato, California, 2011.

20 Frank, D. G.: Mineral Resource Data System (MRDS) data in Arc-View shape file format, for
21 spatial data delivery project, U.S. Geol. Surv., Spokane, Wash., 1999.

22 Friedli, H. R., Radke, L. F., Prescott, R., Li, P., Woo, J. H., and Carmichael, G. R.: Mercury in
23 the atmosphere around Japan, Korea, and China as observed during the 2001 ACE-Asia field
24 campaign: Measurements, distributions, sources, and implications, *J. Geophys. Res.-Atmos.*,
25 109, D19s25, doi:10.1029/2003jd004244, 2004.

26 Friedli, H. R., Arellano, A. F., Cinnirella, S., and Pirrone, N.: Initial estimates of mercury
27 emissions to the atmosphere from global biomass burning, *Environ. Sci. Technol.*, 43,
28 3507-3513, doi:10.1021/es802703g, 2009.

29 Fu, X., Feng, X., Sommar, J., and Wang, S.: A review of studies on atmospheric mercury in
30 China, *Sci. Total Environ.*, 421, 73-81, doi:10.1016/j.scitotenv.2011.09.089, 2012.

31 Ge, B., Wang, Z., Xu, X., Wu, J., Yu, X., and Li, J.: Wet deposition of acidifying substances in
32 different regions of China and the rest of East Asia: Modeling with updated NAQPMS,
33 *Environ. Pollut.*, 187, 10-21, doi:http://dx.doi.org/10.1016/j.envpol.2013.12.014, 2014.

34 Gencarelli, C. N., De Simone, F., Hedgecok, I. M., Sprovieri, F., Pirrone, N.: Development and
35 application of a regional-scale atmospheric mercury model based on WRF/Chem: a
36 Mediterranean area investigation, *Environ. Sci. Pollut. Res.*, 21, 4095-4109, 2014.

37 Granier, C., Lamarque, J. F., Mieville, A., Muller, J. F., and Olivier, J.: POET, a database of
38 surface emissions of ozone precursors , tech. report, available at:
39 <http://www.aero.jussieu.fr/projet/ACCENT/POET.php> (last access: 10 June 2013), 2005.

40 Guenther, A., Karl, T., Harley, P., Wiedinmyer, C., Palmer, P. I., and Geron, C.: Estimates of
41 global terrestrial isoprene emissions using MEGAN (Model of Emissions of Gases and
42 Aerosols from Nature), *Atmos. Chem. Phys.*, 6, 3181-3210, 2006.

43 Hall, B., and Bloom., N.: Report to EPRI, Palo Alto, CA., USA, 1993.

44 Hall, B.: The gas phase oxidation of elemental mercury by ozone, *Water Air Soil Pollut.*, 80,

1 301-315, doi:10.1007/bf01189680, 1995.

2 Harada, M.: Minamata Disease – Methylmercury poisoning in Japan caused by environmental
3 pollution, *Crit. Rev. Toxicol.*, 25, 1-24, doi:10.3109/10408449509089885, 1995.

4 Holmes, C. D., Jacob, D. J., Corbitt, E. S., Mao, J., Yang, X., Talbot, R., and Slemr, F.: Global
5 atmospheric model for mercury including oxidation by bromine atoms, *Atmos. Chem. Phys.*,
6 10, 12037-12057, doi:10.5194/acp-10-12037-2010, 2010.

7 Horowitz, L. W., Walters, S., Mauzerall, D. L., Emmons, L. K., Rasch, P. J., Granier, C., Tie, X.
8 X., Lamarque, J. F., Schultz, M. G., Tyndall, G. S., Orlando, J. J., and Brasseur, G. P.: A global
9 simulation of tropospheric ozone and related tracers: Description and evaluation of MOZART,
10 version 2, *J. Geophys. Res.-Atmos.*, 108, 4784, doi:10.1029/2002jd002853, 2003.

11 Jaffe, D., Prestbo, E., Swartzendruber, P., Weiss-Penzias, P., Kato, S., Takami, A., Hatakeyama,
12 S., and Kajii, Y.: Export of atmospheric mercury from Asia, *Atmos. Environ.*, 39, 3029-3038,
13 doi:10.1016/j.atmosenv.2005.01.030, 2005.

14 Jaffe, D., and Strode, S.: Sources, fate and transport of atmospheric mercury from Asia, *Environ.*
15 *Chem.*, 5, 121-126, doi:10.1071/en08010, 2008.

16 Jiang, G., Shi, J., and Feng, X.: Mercury pollution in China: An overview of the past and current
17 sources of the toxic metal, *Environ. Sci. Technol.*, 40, 3673-3678, 2006.

18 Jung, G., Hedgecock, I. M., and Pirrone, N.: ECHMERIT V1.0-a new global fully coupled
19 mercury-chemistry and transport model, *Geosci. Model Dev.*, 2, 175-195, 2009.

20 Keeler, G. J., Pirrone, N., Bullock, R., and Sillman, S.: The need for a coordinated global Hg
21 monitoring network for global and regional models validation, in: *Mercury Fate and Transport*
22 *in the Global Atmosphere*, edited by: Mason, R., and Pirrone, N., Springer, USA, 391-424,
23 2009.

24 Lamarque, J. F., Bond, T. C., Eyring, V., Granier, C., Heil, A., Klimont, Z., Lee, D., Liousse, C.,
25 Mieville, A., Owen, B., Schultz, M. G., Shindell, D., Smith, S. J., Stehfest, E., Van Aardenne,
26 J., Cooper, O. R., Kainuma, M., Mahowald, N., McConnell, J. R., Naik, V., Riahi, K., and van
27 Vuuren, D. P.: Historical (1850-2000) gridded anthropogenic and biomass burning emissions
28 of reactive gases and aerosols: methodology and application, *Atmos. Chem. Phys.*, 10,
29 7017-7039, doi:10.5194/acp-10-7017-2010, 2010.

30 Lamborg, C. H., Fitzgerald, W. F., O'Donnell, J., and Torgersen, T.: A non-steady-state
31 compartmental model of global-scale mercury biogeochemistry with interhemispheric
32 atmospheric gradients, *Geochim. Cosmochim. Ac.*, 66, 1105-1118,
33 doi:10.1016/s0016-7037(01)00841-9, 2002.

34 Lawrence, M. G., Jöckel, P., and von Kuhlmann, R.: What does the global mean OH
35 concentration tell us?, *Atmos. Chem. Phys.*, 1, 37-49, doi:10.5194/acp-1-37-2001, 2001.

36 Lei, H., Liang, X., Wuebbles, D. J., and Tao, Z.: Model analyses of atmospheric mercury: present
37 air quality and effects of transpacific transport on the United States, *Atmos. Chem. Phys.*, 13,
38 10807-10825, doi:10.5194/acp-13-10807-2013, 2013.

39 Li, J., Wang, Z., Akimoto, H., Gao, C., Pochanart, P., and Wang, X.: Modeling study of ozone
40 seasonal cycle in lower troposphere over east Asia, *J. Geophys. Res.-Atmos.*, 112, D22s25,
41 doi:10.1029/2006jd008209, 2007.

42 Li, J., Wang, Z., Wang, X., Yamaji, K., Takigawa, M., Kanaya, Y., Pochanart, P., Liu, Y., Irie, H.,
43 Hu, B., Tanimoto, H., and Akimoto, H.: Impacts of aerosols on summertime tropospheric
44 photolysis frequencies and photochemistry over Central Eastern China, *Atmos. Environ.*, 45,

1 1817-1829, doi:10.1016/j.atmosenv.2011.01.016, 2011.

2 Li, J., Wang, Z., Zhuang, G., Luo, G., Sun, Y., and Wang, Q.: Mixing of Asian mineral dust with
3 anthropogenic pollutants over East Asia: a model case study of a super-duststorm in March
4 2010, *Atmos. Chem. Phys.*, 12, 7591-7607, doi:10.5194/acp-12-7591-2012, 2012.

5 Liang, S., Xu, M., Liu, Z., Suh, S. and Zhang T.: Socioeconomic Drivers of Mercury Emissions
6 in China from 1992 to 2007, *Environ. Sci. Technol.*, 47(7): 3234-3240, 2013.

7 Lin, C. J., and Pehkonen, S. O.: Aqueous free radical chemistry of mercury in the presence of
8 iron oxides and ambient aerosol, *Atmos. Environ.*, 31, 4125-4137,
9 doi:http://dx.doi.org/10.1016/S1352-2310(97)00269-0, 1997.

10 Lin, C. J., and Pehkonen, S. O.: Oxidation of elemental mercury by aqueous chlorine
11 (HOCl/OCl⁻): Implications for tropospheric mercury chemistry, *J. Geophys. Res.-Atmos.*, 103,
12 28093-28102, doi:10.1029/98jd02304, 1998.

13 Lin, C. J., Pongprueksa, P., Lindberg, S. E., Pehkonen, S. O., Byun, D., and Jang, C.: Scientific
14 uncertainties in atmospheric mercury models I: Model science evaluation, *Atmos. Environ.*, 40,
15 doi:2911-2928, 10.1016/j.atmosenv.2006.01.009, 2006.

16 Lin, C. J., and Pehkonen, S. O.: The chemistry of atmospheric mercury: a review, *Atmos.*
17 *Environ.*, 33, 2067-2079, doi:10.1016/s1352-2310(98)00387-2, 1999.

18 Lin, C. J., Pongprueks, P., Ho, T. C., and Jang, C.: Development of mercury modeling schemes
19 within CMAQ framework: Science and model implementation issues, In: Proceedings of the
20 2004 CMAS Models-3 Conference, Research Triangle Park, NC, October 18-20 (CD-ROM).
21 2004.

22 Lindberg, S., Bullock, R., Ebinghaus, R., Engstrom, D., Feng, X., Fitzgerald, W., Pirrone, N.,
23 Prestbo, E., and Seigneur, C.: A synthesis of progress and uncertainties in attributing the
24 sources of mercury in deposition, *Ambio*, 36, 19-32, 2007.

25 Lindqvist, O., and Rodhe, H.: Atmospheric mercury – A review, *Tellus B*, 37, 136-159, 1985.

26 Mason, R.: Mercury emissions from natural processes and their importance in the global mercury
27 cycle, in: *Mercury Fate and Transport in the Global Atmosphere*, edited by: Mason, R., and
28 Pirrone, N., Springer, USA, 173-191, 2009.

29 Munthe, J.: The aqueous oxidation of elemental mercury by ozone, *Atmos. Environ.*, 26,
30 1461-1468, doi:10.1016/0960-1686(92)90131-4, 1992.

31 Pacyna, E. G., Pacyna, J. M., Steenhuisen, F., and Wilson, S.: Global anthropogenic mercury
32 emission inventory for 2000, *Atmos. Environ.*, 40, 4048-4063,
33 doi:http://dx.doi.org/10.1016/j.atmosenv.2006.03.041, 2006.

34 Pan, L., Chai, T., Carmichael, G. R., Tang, Y., Streets, D., Woo, J.-H., Friedli, H. R., and Radke,
35 L. F.: Top-down estimate of mercury emissions in China using four-dimensional variational
36 data assimilation, *Atmos. Environ.*, 41, 2804-2819,
37 doi:http://dx.doi.org/10.1016/j.atmosenv.2006.11.048, 2007.

38 Pan, L., Carmichael, G. R., Adhikary, B., Tang, Y., Streets, D., Woo, J.-H., Friedli, H. R., and
39 Radke, L. F.: A regional analysis of the fate and transport of mercury in East Asia and an
40 assessment of major uncertainties, *Atmos. Environ.*, 42, 1144-1159,
41 doi:10.1016/j.atmosenv.2007.10.045, 2008.

42 Pehkonen, S. O., and Lin, C. J.: Aqueous photochemistry of mercury with organic acids, *J. Air*
43 *Waste Manage. Assoc.*, 48, 144-150, doi:10.1080/10473289.1998.10463661, 1998.

44 Pirrone, N., Cinnirella, S., Feng, X., Finkelman, R. B., Friedli, H. R., Leaner, J., Mason, R.,

1 Mukherjee, A. B., Stracher, G. B., Streets, D. G., and Telmer, K.: Global mercury emissions to
2 the atmosphere from anthropogenic and natural sources, *Atmos. Chem. Phys.*, 10, 5951-5964,
3 doi:10.5194/acp-10-5951-2010, 2010.

4 Pirrone, N., and Keating, T.: *Hemispheric Transport of Air Pollution 2010 Part B: Mercury*,
5 United Nations, New York and Geneva, 210 pp., 2010.

6 Price, C., Penner, J., and Prather, M.: NO_x from lightning: 1. Global distribution based on
7 lightning physics, *J. Geophys. Res.-Atmos.*, 102, 5929-5941, doi:10.1029/96jd03504, 1997.

8 Ryaboshapko, A., Bullock, O. R., Jr., Christensen, J., Cohen, M., Dastoor, A., Ilyin, I., Petersen,
9 G., Syrakov, D., Travnikov, O., Artz, R. S., Davignon, D., Draxler, R. R., Munthe, J., and
10 Pacyna, J.: Intercomparison study of atmospheric mercury models: 2. Modelling results vs.
11 long-term observations and comparison of country deposition budgets, *Sci. Total Environ.*,
12 377, 319-333, doi:10.1016/j.scitotenv.2007.01.071, 2007.

13 Sanemasa, I.: The solubility of elemental mercury vapor in water, *Bull. Chem. Soc. Jpn.*, 48,
14 1795-1798, 1975.

15 Schroeder, W. H., Anlauf, K. G., Barrie, L. A., Lu, J. Y., Steffen, A., Schneeberger, D. R., and
16 Berg, T.: Arctic springtime depletion of mercury, *Nature*, 394, 331-332, doi:10.1038/28530,
17 1998.

18 Schroeder, W. H., and Munthe, J.: Atmospheric mercury - An overview, *Atmos. Environ.*, 32,
19 809-822, doi:10.1016/s1352-2310(97)00293-8, 1998.

20 Seigneur, C., Abeck, H., Chia, G., Reinhard, M., Bloom, N. S., Prestbo, E., and Saxena, P.:
21 Mercury adsorption to elemental carbon (soot) particles and atmospheric particulate matter,
22 *Atmos. Environ.*, 32, 2649-2657, doi:http://dx.doi.org/10.1016/S1352-2310(97)00415-9, 1998.

23 Seigneur, C., Karamchandani, P., Lohman, K., Vijayaraghavan, K., and Shia, R. L.: Multiscale
24 modeling of the atmospheric fate and transport of mercury, *J. Geophys. Res.-Atmos.*, 106,
25 27795-27809, doi:10.1029/2000jd000273, 2001.

26 Seigneur, C., Vijayaraghavan, K., Lohman, K., Karamchandani, P., and Scott, C.: Global source
27 attribution for mercury deposition in the United States, *Environ. Sci. Technol.*, 38, 555-569,
28 doi:10.1021/es034109t, 2004.

29 Selin, N. E., Jacob, D. J., Park, R. J., Yantosca, R. M., Strode, S., Jaegle, L., and Jaffe, D.:
30 Chemical cycling and deposition of atmospheric mercury: Global constraints from
31 observations, *J. Geophys. Res.-Atmos.*, 112, D02308, doi:10.1029/2006jd007450, 2007.

32 Selin, N. E., Jacob, D. J., Yantosca, R. M., Strode, S., Jaegle, L., and Sunderland, E. M.: Global
33 3-D land-ocean-atmosphere model for mercury: Present-day versus preindustrial cycles and
34 anthropogenic enrichment factors for deposition, *Global Biogeochem. Cy.*, 22, Gb3099,
35 doi:10.1029/2008gb003282, 2008.

36 Selin, N. E.: Global biogeochemical cycling of mercury: A review, *Annu. Rev. Environ. Resour.*,
37 34, 43, 2009.

38 Sillen, L. G., Martell, A. E., and Bjerrum, J.: Stability constants of metal-ion complexes, *Chem.*
39 *Soc.*, 17, 754, 1964.

40 Soerensen, A. L., Skov, H., Jacob, D. J., Soerensen, B. T., and Johnson, M. S.: Global
41 concentrations of gaseous elemental mercury and reactive gaseous mercury in the marine
42 boundary layer, *Environ. Sci. Technol.*, 44, 7425-7430, doi:10.1021/es903839n, 2010a.

43 Soerensen, A. L., Sunderland, E. M., Holmes, C. D., Jacob, D. J., Yantosca, R. M., Skov, H.,
44 Christensen, J. H., Strode, S. A., and Mason, R. P.: An improved global model for air-sea

1 exchange of mercury: High concentrations over the North Atlantic, *Environ. Sci. Technol.*, 44,
2 8574-8580, doi:10.1021/es102032g, 2010b.

3 Soerensen, A. L., Jacob, D. J., Streets, D., Witt, M., Ebinghaus, R., Mason, R. P., Andersson, M.
4 and Sunderland E. M.: Multi-decadal decline of mercury in the North Atlantic atmosphere
5 explained by changing subsurface seawater concentrations, *Geophys. Res. Lett.* 39: Art
6 #L21810, 2012.

7 Sommar, J., Gardfeldt, K., Stromberg, D., and Feng, X. B.: A kinetic study of the gas-phase
8 reaction between the hydroxyl radical and atomic mercury, *Atmos. Environ.*, 35, 3049-3054,
9 doi:10.1016/s1352-2310(01)00108-x, 2001.

10 Song, S., Selin, N. E., Soerensen, A. L., Angot, H., Artz, R., Brooks, S., Brunke, E.-G., Conley,
11 G., Dommergue, A., Ebinghaus, R., Holsen, T. M., Jaffe, D. A., Kang, S., Kelley, P., Luke, W.
12 T., Magand, O., Marumoto, K., Pfaffhuber, K. A., Ren, X., Sheu, G.-R., Slemr, F., Warneke, T.,
13 Weigelt, A., Weiss-Penzias, P., Wip, D. C., and Zhang, Q.: Top-down constraints on
14 atmospheric mercury emissions and implications for global biogeochemical cycling, *Atmos.*
15 *Chem. Phys.*, 15, 7103-7125, doi:10.5194/acp-15-7103-2015, 2015.

16 Sprovieri, F., Pirrone, N., Ebinghaus, R., Kock, H., and Dommergue, A.: A review of worldwide
17 atmospheric mercury measurements, *Atmos. Chem. Phys.*, 10, 8245-8265,
18 doi:10.5194/acp-10-8245-2010, 2010.

19 Steffen, A., Schroeder, W., Macdonald, R., Poissant, L., and Konoplev, A.: Mercury in the Arctic
20 atmosphere: An analysis of eight years of measurements of GEM at Alert (Canada) and a
21 comparison with observations at Amderma (Russia) and Kuujjuarapik (Canada), *Sci. Total*
22 *Environ.*, 342, 185-198, doi:10.1016/j.scitotenv.2004.12.048, 2005.

23 Strode, S. A., Jaegle, L., Selin, N. E., Jacob, D. J., Park, R. J., Yantosca, R. M., Mason, R. P., and
24 Slemr, F.: Air-sea exchange in the global mercury cycle, *Global Biogeochem. Cy.*, 21, Gb1017,
25 doi:10.1029/2006gb002766, 2007.

26 Strode, S. A., Jaegle, L., Jaffe, D. A., Swartzendruber, P. C., Selin, N. E., Holmes, C., and
27 Yantosca, R. M.: Trans-Pacific transport of mercury, *J. Geophys. Res.-Atmos.*, 113, D15305,
28 doi:10.1029/2007jd009428, 2008.

29 Tang, X., Wang, Z., Zhu, J., Gbaguidi, A. E., Wu, Q., Li, J., and Zhu, T.: Sensitivity of ozone to
30 precursor emissions in urban Beijing with a Monte Carlo scheme, *Atmos. Environ.*, 44,
31 3833-3842, doi:http://dx.doi.org/10.1016/j.atmosenv.2010.06.026, 2010.

32 Taylor, K. E.: Summarizing multiple aspects of model performance in a single diagram, *J.*
33 *Geophys. Res.-Atmos.*, 106, 7183-7192, doi:10.1029/2000jd900719, 2001.

34 Temme, C., Slemr, F., Ebinghaus, R., and Einax, J. W.: Distribution of mercury over the Atlantic
35 Ocean in 1996 and 1999-2001, *Atmos. Environ.*, 37, 1889-1897,
36 doi:10.1016/s1352-2310(03)00069-4, 2003.

37 Tokos, J. J. S., Hall, B., Calhoun, J. A., and Prestbo, E. M.: Homogeneous gas-phase reaction of
38 Hg⁰ with H₂O₂, O₃, CH₃I, and (CH₃)₂S: Implications for atmospheric Hg cycling, *Atmos.*
39 *Environ.*, 32, 823-827, doi:10.1016/s1352-2310(97)00171-4, 1998.

40 Travnikov, O.: Contribution of the intercontinental atmospheric transport to mercury pollution in
41 the Northern Hemisphere, *Atmos. Environ.*, 39, 7541-7548,
42 doi:10.1016/j.atmosenv.2005.07.066, 2005.

43 Travnikov, O., and Ilyin, I.: The EMEP/MSC-E mercury modeling system, in: *Mercury Fate and*
44 *Transport in the Global Atmosphere*, edited by: Mason, R., and Pirrone, N., Springer, USA,

1 571-587, 2009.

2 Van Loon, L., Mader, E., and Scott, S. L.: Reduction of the aqueous mercuric ion by sulfite: UV
3 spectrum of HgSO_3 and its intramolecular redox reaction, *J. Phys. Chem. A*, 104, 1621-1626,
4 doi:10.1021/jp994268s, 2000.

5 Van Loon, L. L., Mader, E. A., and Scott, S. L.: Sulfite stabilization and reduction of the aqueous
6 mercuric ion: Kinetic determination of sequential formation constants, *J. Phys. Chem. A*, 105,
7 3190-3195, doi:10.1021/jp003803h, 2001.

8 Vijayaraghavan, K., P. Karamchandani, C. Seigneur, R. Balmori, and S.-Y. Chen: Plume-in-grid
9 modeling of atmospheric mercury, *J. Geophys. Res.*, 113, D24305,
10 doi:10.1029/2008JD010580, 2008.

11 Voulgarakis, A., Naik, V., Lamarque, J. F., Shindell, D. T., Young, P. J., Prather, M. J., Wild, O.,
12 Field, R. D., Bergmann, D., Cameron-Smith, P., Cionni, I., Collins, W. J., Dalsøren, S. B.,
13 Doherty, R. M., Eyring, V., Faluvegi, G., Folberth, G. A., Horowitz, L. W., Josse, B.,
14 MacKenzie, I. A., Nagashima, T., Plummer, D. A., Righi, M., Rumbold, S. T., Stevenson, D. S.,
15 Strode, S. A., Sudo, K., Szopa, S., and Zeng, G.: Analysis of present day and future OH and
16 methane lifetime in the ACCMIP simulations, *Atmos. Chem. Phys.*, 13, 2563-2587,
17 doi:10.5194/acp-13-2563-2013, 2013.

18 Walcek, C. J., and Aleksic, N. M.: A simple but accurate mass conservative, peak-preserving,
19 mixing ratio bounded advection algorithm with Fortran code, *Atmos. Environ.*, 32, 3863-3880,
20 doi:10.1016/s1352-2310(98)00099-5, 1998.

21 Wang, Q., Fu, Q., Wang, Z., Wang, T., Liu, P., Lu, T., Duan, Y., and Huang, Y.: Application of
22 ensemble numerical model system on the air quality forecast in Shanghai (in Chinese),
23 *Environmental Monitoring and Forewarning*, 2(4), 1-6+11, 2010.

24 Wang, Z., Akimoto, H., and Uno, I.: Neutralization of soil aerosol and its impact on the
25 distribution of acid rain over east Asia: Observations and model results, *J. Geophys.*
26 *Res.-Atmos.*, 107, 4389, doi:10.1029/2001jd001040, 2002.

27 Wang, Z., Xie, F., Wang, X., An, J., and Zhu, J.: Development and application of Nested Air
28 Quality Prediction Modeling System (in Chinese), *Chinese Journal of Atmospheric Sciences*,
29 30(5), 778-790, 2006.

30 Wang, Z., Wu, Q., Gbaguidi, A., Yan, P., Zhang, W., Wang, W., and Tang, X.: Ensemble air
31 quality multi-model forecast system for Beijing (EMS-Beijing): Model description and
32 preliminary application (in Chinese), *Journal of Nanjing University of Information Science &*
33 *Technology (Natural Science Edition)*, 1(1), 19-26, 2009.

34 Wesely, M. L.: Parameterization of surface resistances to gaseous dry deposition in
35 regional-scale numerical models, *Atmos. Environ.*, 23, 1293-1304,
36 doi:http://dx.doi.org/10.1016/0004-6981(89)90153-4, 1989.

37 Wilson, S. J., Steenhuisen, F., Pacyna, J. M., and Pacyna, E. G.: Mapping the spatial distribution
38 of global anthropogenic mercury atmospheric emission inventories, *Atmos. Environ.*, 40,
39 4621-4632, doi:http://dx.doi.org/10.1016/j.atmosenv.2006.03.042, 2006.

40 Wu, Q., Wang, Z., Chen, H., Zhou, W., and Wenig, M.: An evaluation of air quality modeling
41 over the Pearl River Delta during November 2006, *Meteorol. Atmos. Phys.*, 116, 113-132,
42 doi:10.1007/s00703-011-0179-z, 2012.

43 Yan, X., Ohara, T., and Akimoto, H.: Statistical modeling of global soil NO_x emissions, *Global*
44 *Biogeochem. Cy.*, 19, 2005.

- 1 Zhang, Y., Jaegle, L., van Donkelaar, A., Martin, R. V., Holmes, C. D., Amos, H. M., Wang, Q.,
2 Talbot, R., Artz, R., Brooks, S., Luke, W., Holsen, T. M., Felton, D., Miller, E. K., Perry, K. D.,
3 Schmeltz, D., Steffen, A., Tordon, R., Weiss-Penzias, P., and Zsolway, R.: Nested-grid
4 simulation of mercury over North America, *Atmos. Chem. Phys.*, 12, 6095-6111,
5 doi:10.5194/acp-12-6095-2012, 2012.
- 6 Zaveri, R., and Peters, L.: A new lumped structure photochemical mechanism for large-scale
7 applications, *J. Geophys. Res.-Atmos.*, 104, 30387-30415,1999.
- 8

Table 1. Reactions and rate constants used in the GNAQPMS-Hg model.

NO.	Reaction	Rates (k or K) ^a	References
Gas-phase reactions			
RG1	Hg(0)(g)+O ₃ (g)→Hg(II)(g)	3x10 ⁻²⁰ cm ³ molec ⁻¹ s ⁻¹	Hall (1995)
RG2	Hg(0)(g)+HCl(g)→HgCl ₂ (g)	1x10 ⁻¹⁹ cm ³ molec ⁻¹ s ⁻¹	Hall and Bloom (1993)
RG3	Hg(0)(g)+H ₂ O ₂ (g)→Hg(OH) ₂ (g)	8.5x10 ⁻¹⁹ cm ³ molec ⁻¹ s ⁻¹	Tokos et al. (1998)
RG4	Hg(0)(g)+Cl ₂ (g)→HgCl ₂ (g)	2.6x10 ⁻¹⁸ cm ³ molec ⁻¹ s ⁻¹	Ariya et al. (2002)
RG5	Hg(0)(g)+OH(g)→Hg(OH) ₂ (g)	8x10 ⁻¹⁴ cm ³ molec ⁻¹ s ⁻¹	Sommar et al. (2001)
Gas-liquid equilibria			
GL1	Hg(0)(g)↔Hg(0)(aq)	0.11 M atm ⁻¹	Sanemasa (1975)
GL2	HgCl ₂ (g)↔HgCl ₂ (aq)	1.4x10 ⁶ M atm ⁻¹	Lindqvist and Rodhe (1985)
GL3	Hg(OH) ₂ (g)↔Hg(OH) ₂ (aq)	1.2x10 ⁴ M atm ⁻¹	Lindqvist and Rodhe (1985)
Aqueous-phase equilibria			
AE1	HgCl ₂ (aq)↔Hg ²⁺ +2Cl ⁻	1x10 ⁻¹⁴ M ²	Sillen et al. (1964)
AE2	Hg(OH) ₂ (aq)↔Hg ²⁺ +2OH ⁻	1x10 ⁻²² M ²	Sillen et al. (1964)
AE3	Hg ²⁺ +SO ₃ ²⁻ ↔HgSO ₃	2.1x10 ¹³ M ⁻¹	Van Loon et al. (2001)
AE4	HgSO ₃ +SO ₃ ²⁻ ↔Hg(SO ₃) ₂ ⁻	1x10 ¹⁰ M ⁻¹	Van Loon et al. (2001)
Aqueous-phase reaction			
RA1	Hg(0)(aq)+O ₃ (aq)→Hg ²⁺	4.7x10 ⁷ M ⁻¹ s ⁻¹	Munthe (1992)
RA2	Hg(0)(aq)+OH(aq)→Hg ²⁺	2x10 ⁹ M ⁻¹ s ⁻¹	Lin and Pehkonen (1997)
RA3	HgSO ₃ (aq)→Hg(0)(aq)	0.0106 s ⁻¹	Van Loon et al. (2000)
RA4	Hg(II)(aq)+HO ₂ (aq)→Hg(0)(aq)	1.7x10 ⁴ M ⁻¹ s ⁻¹	Pehkonen and Lin (1998)
RA5	Hg(0)(aq)+HOCl(aq)→Hg ²⁺	2.09x10 ⁶ M ⁻¹ s ⁻¹	Lin and Pehkonen (1998)
RA6	Hg(0)(aq)+OCl ⁻ →Hg ²⁺	1.99x10 ⁶ M ⁻¹ s ⁻¹	Lin and Pehkonen (1998)
Adsorption of Hg(II) on PM in the aqueous-phase			
AD1	Hg(II)(aq)↔Hg(II)(p)	34 L g ⁻¹	Seigneur et al. (1998)

^a The reaction rate constants are for temperatures in the range of 20 to 25⁰C. No temperature dependence information is available.

Table 2. Global budgets of TGM in the literature (Unit: Mg yr⁻¹).

	Bergan et al. (1999)	Shia et al. (1999)	Lamborg et al. (2002)	Mason et al. (2002)	Seigneur et al. (2004)	Selin et al. (2007)	Selin et al. (2008)	This work
Total Sources	6050	6100	4400	6600	6411	7000	11200	10163
anthropogenic	2150	2100	2600	2400	2143	2200	3400	2488
land	2500	2000	1000	1600	2290	2000	2800	2675
ocean	1400	2000	800	2600	1978	2800	5000	5000
Total Sinks	6050	6100	4200	6600	6411	7000	11200	10163
Wet deposition		2800		3920		2100		2283
Dry deposition		3300		2680		4700		7880
TGM Burden	6050	10400	5220	5000	7690	5360	5600	5507
TGM lifetime(yr)	1	1.7	1.3	0.76	1.2	0.79	0.5	0.54

Table 3. Statistical summary of comparisons of the model results with observations^a.

Parameter	Region	R	NMB	RMSE	SVR ^b
TGM	East Asia Nested	0.51	-39%	3.87	2.56
	East Asia	0.54	-32%	3.61	2.56
	North America	0.69	18%	0.58	0.48
	Europe	0.57	-8%	0.17	0.35
	Global	0.70	-18%	2.22	-
Oxidized mercury	East Asia Nested	0.45	-12%	242	3.66
	East Asia	0.31	-10%	259	3.66
	North America	0.53	148%	28	1.61
	Europe	0.91	155%	48	1.00
	Global	0.53	3%	185	-
Wet deposition	East Asia Nested	0.78	-28%	45.5	6.69
	East Asia	0.36	-61%	60.1	6.69
	North America	0.76	-4%	4.3	1.89
	Europe	0.78	4%	1.5	1.40
	Global	0.38	-36%	29.3	-
Dry deposition	East Asia Nested	0.88	-42%	87.0	-
	East Asia	0.81	-42%	88.5	-

^a R, NMB, RMSE, SVR represent correlation coefficient, normalized mean bias, root mean square error, spatial variation ratio. Units of TGM, oxidized mercury, wet and dry deposition are ng m^{-3} , pg m^{-3} , $\mu\text{g m}^{-2} \text{yr}^{-1}$, $\mu\text{g m}^{-2} \text{yr}^{-1}$ respectively.

^b SVR defines as (max-min)/mean observations over all sites.

Table 4. Statistical comparisons of the online and offline nested simulation results with observations over East Asia^a.

Parameter	Case ^b	<i>R</i>	NMB	RMSE
TGM	Base simulation	0.51	-39%	3.87
	3 hour boundary conditions	0.50	-42%	3.94
	6 hour boundary conditions	0.50	-42%	3.95
Oxidized mercury	Base simulation	0.45	-12%	242.15
	3 hour boundary conditions	0.42	-17%	251.52
	6 hour boundary conditions	0.41	-18%	252.78
Wet deposition	Base simulation	0.78	-28%	45.47
	3 hour boundary conditions	0.78	-29%	45.75
	6 hour boundary conditions	0.78	-29%	45.78
Dry deposition	Base simulation	0.88	-42%	87.02
	3 hour boundary conditions	0.88	-44%	88.55
	6 hour boundary conditions	0.87	-45%	88.96

^a *R*, NMB, RMSE represent correlation coefficient, normalized mean bias, root mean square error. Units of TGM, oxidized mercury, wet and dry deposition are ng m⁻³, pg m⁻³, μg m⁻² yr⁻¹, μg m⁻² yr⁻¹ respectively.

^b In the base simulation, the nested domain gets boundary conditions from the global domain every 10 minutes.

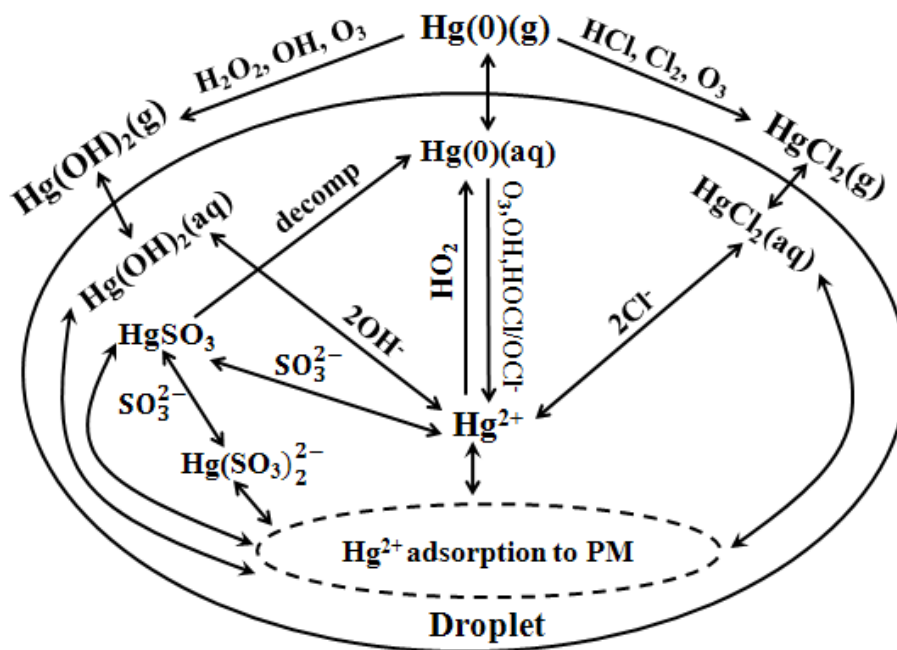


Fig. 1. Schematic of different mercury reactions utilized in the GNAQPMS-Hg model.

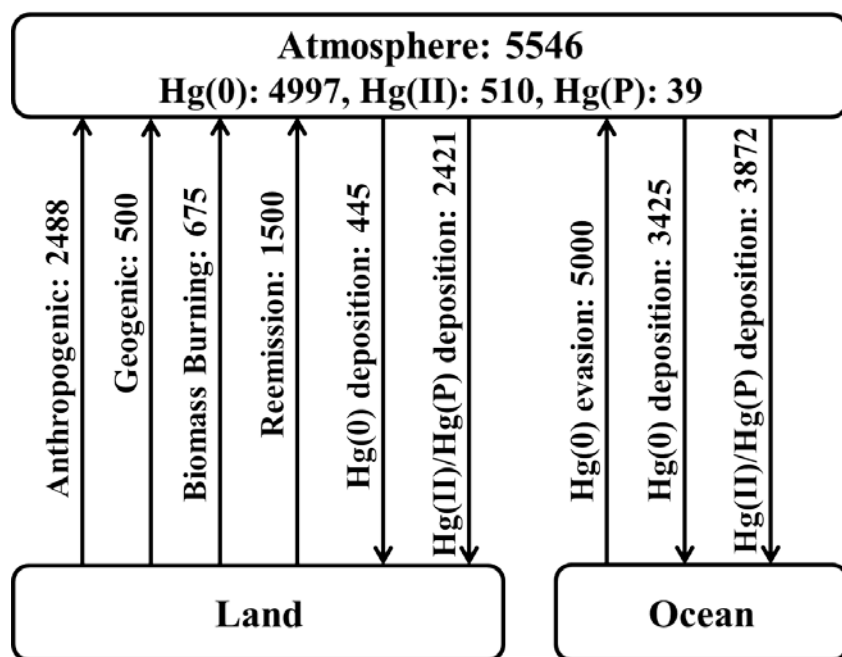


Fig. 2. Global atmospheric mercury budget in GNAQPMS-Hg. Units are Mg yr^{-1} .

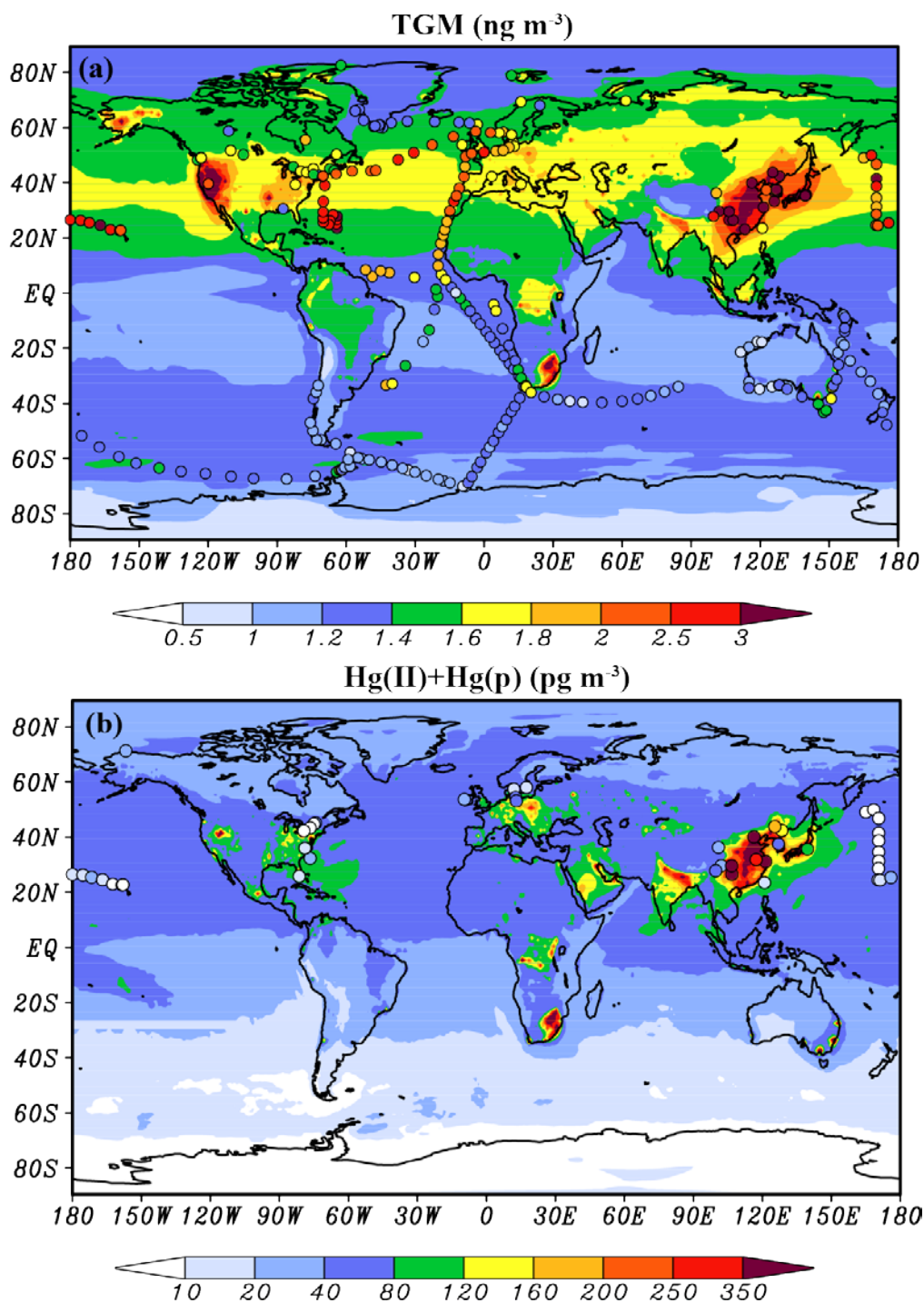


Fig. 3. Annual average TGM (a) and oxidized mercury (Hg(II)+Hg(P) ,b) concentrations in surface air. Model results (background, for year 2001) are compared to observations (circles) from long-term surface sites and short-term ship cruises. Units of TGM and oxidized mercury are ng m^{-3} and pg m^{-3} , respectively.

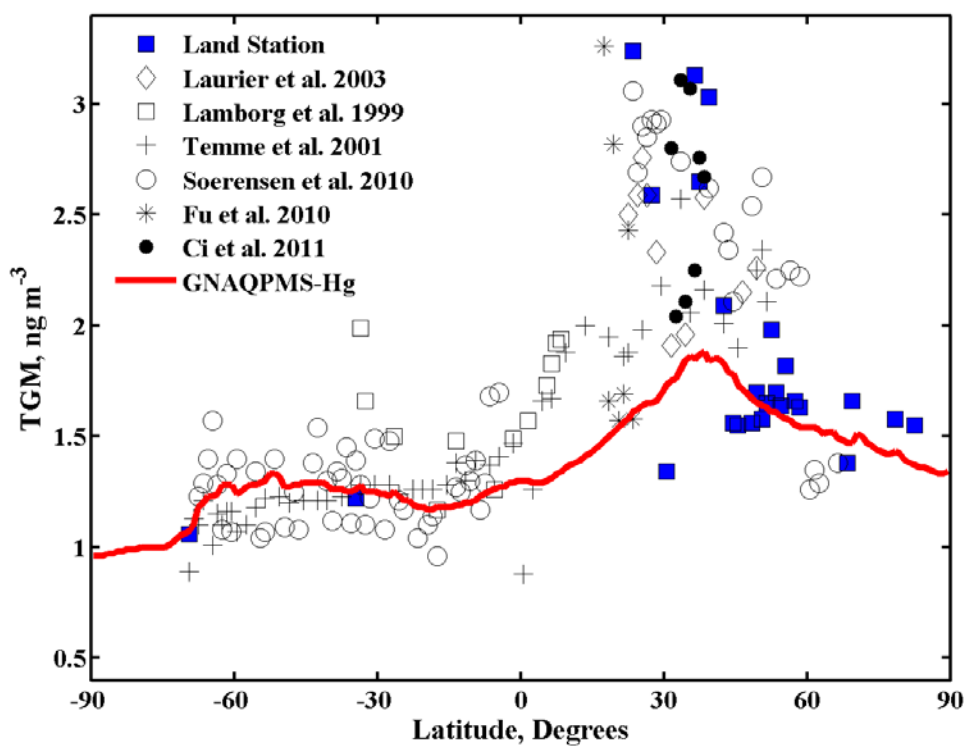


Fig. 4. Variation of surface TGM concentrations (ng m^{-3}) with latitude. Zonally averaged, annual mean model results (line) are compared to observations (symbols).

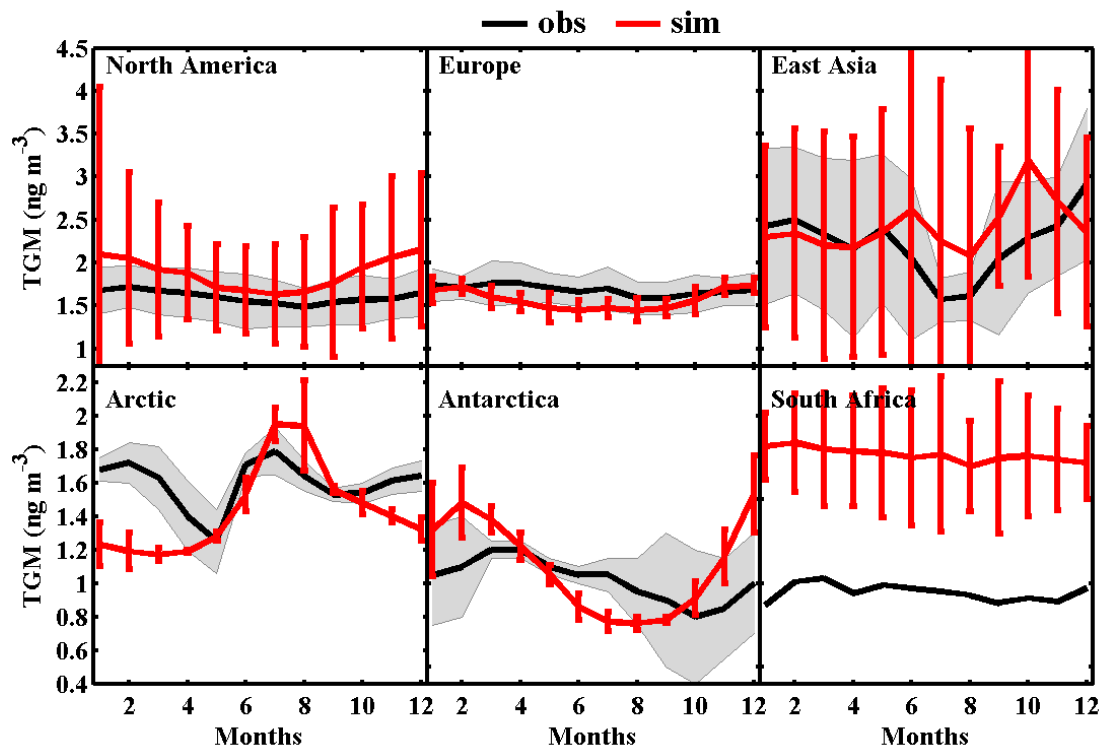


Fig. 5. Mean seasonal variation of TGM (ng m^{-3}) at North America, Europe, East Asia, Arctic, Antarctica and South Africa sites. Gray shaded areas and red vertical bars show one standard deviation over the sites for observations and for model results.

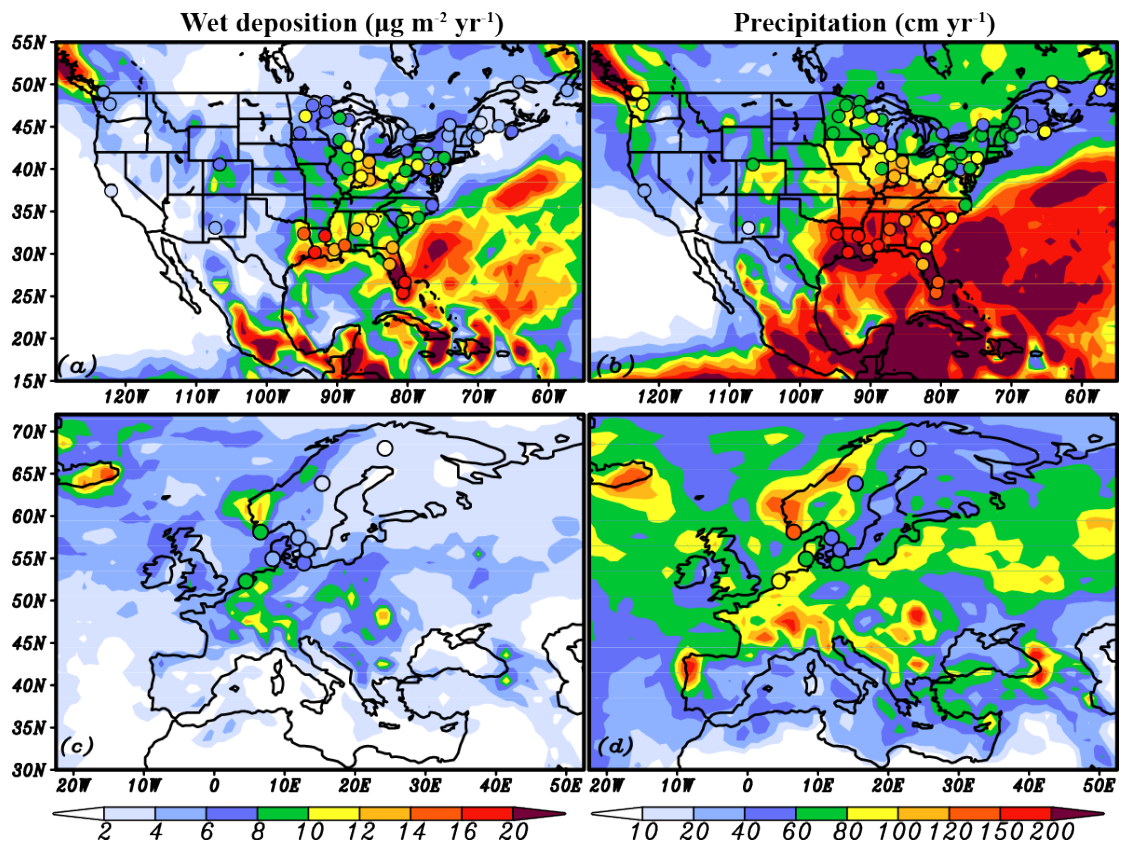


Fig. 6. Simulated annual mercury wet deposition ($\mu\text{g m}^{-2} \text{yr}^{-1}$) and accumulated precipitation (cm yr^{-1}) over North America (a, b) and Europe (c, d) in 2001. Overlaid points show observations for the same year from the Mercury Deposition Network (MDN) over North America, and the European Monitoring and Evaluation Programme (EMEP) over Europe.

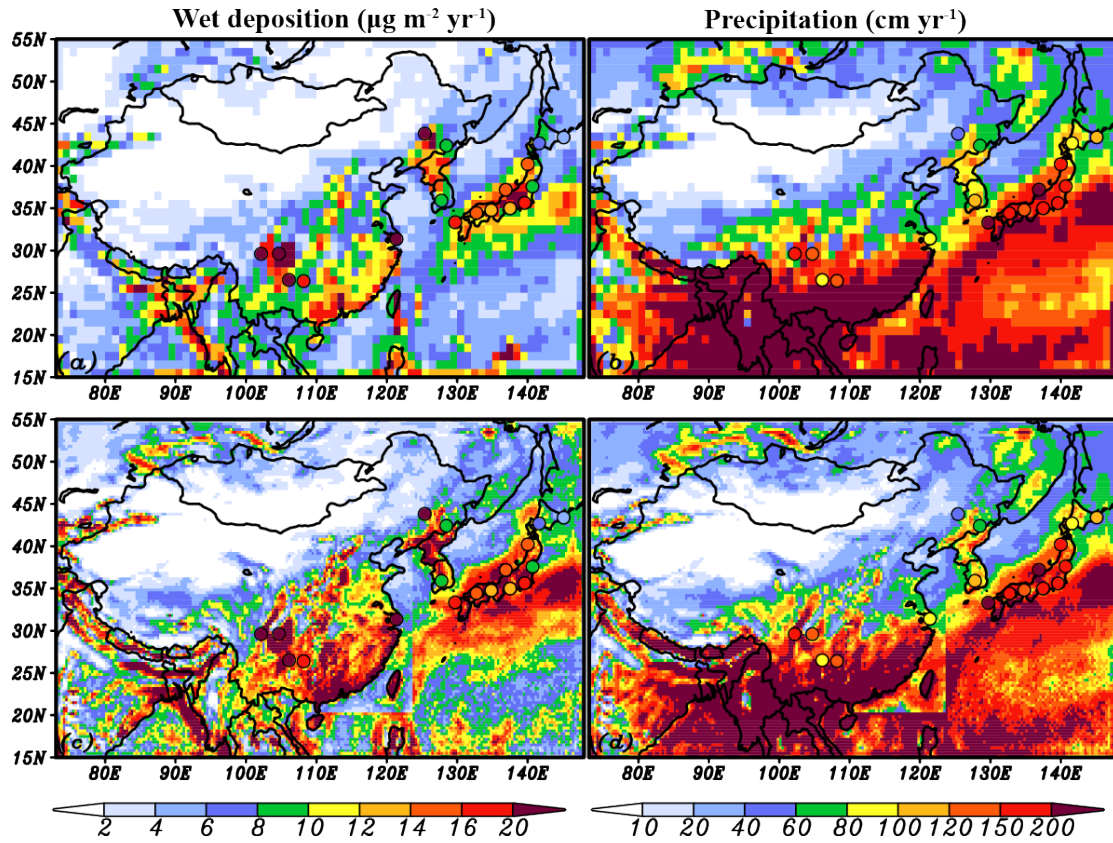


Fig. 7. Simulated annual mercury wet deposition ($\mu\text{g m}^{-2} \text{yr}^{-1}$) and accumulated precipitation (cm yr^{-1}) over East Asia in the global (a, b) and nested (c, d) domains in 2001. Overlaid points show observations collected from the literature. Note that observations and simulated results are not in the same year.

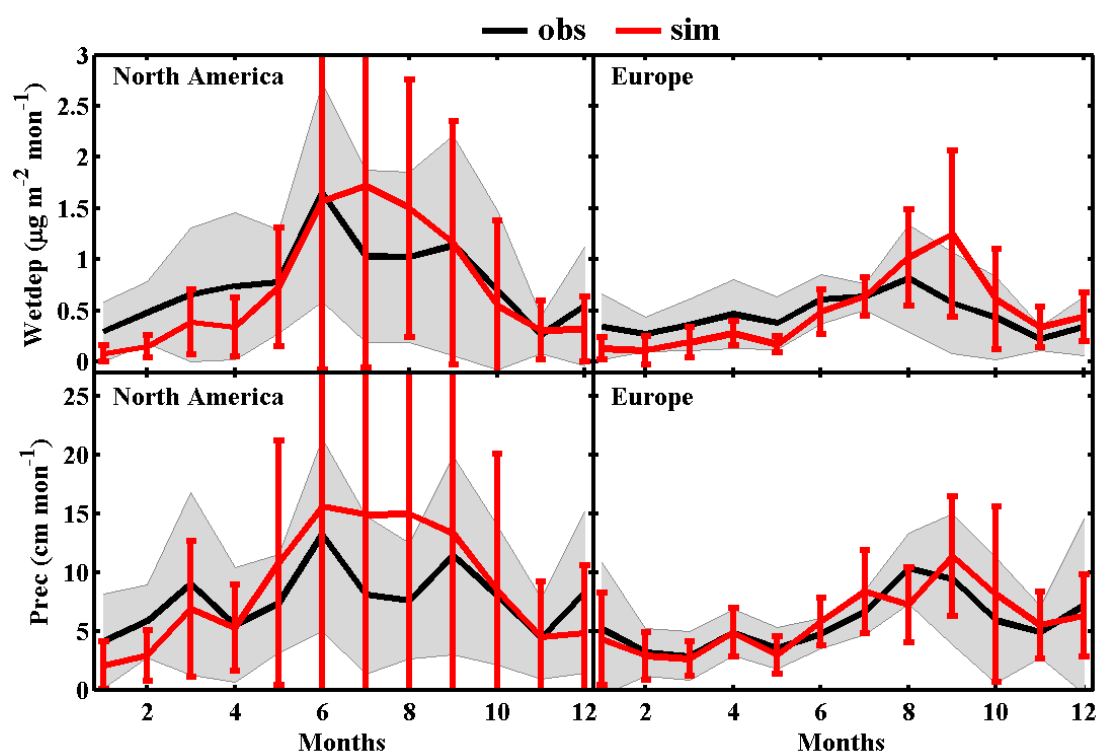


Fig. 8. Mean seasonal variation of mercury wet deposition ($\mu\text{g m}^{-2} \text{mon}^{-1}$) and accumulated precipitation (cm mon^{-1}) at North America (51 sites averaged) and Europe (8 sites averaged) sites in 2001. Gray shaded areas and red vertical bars show one standard deviation over the sites for observations and for model results.

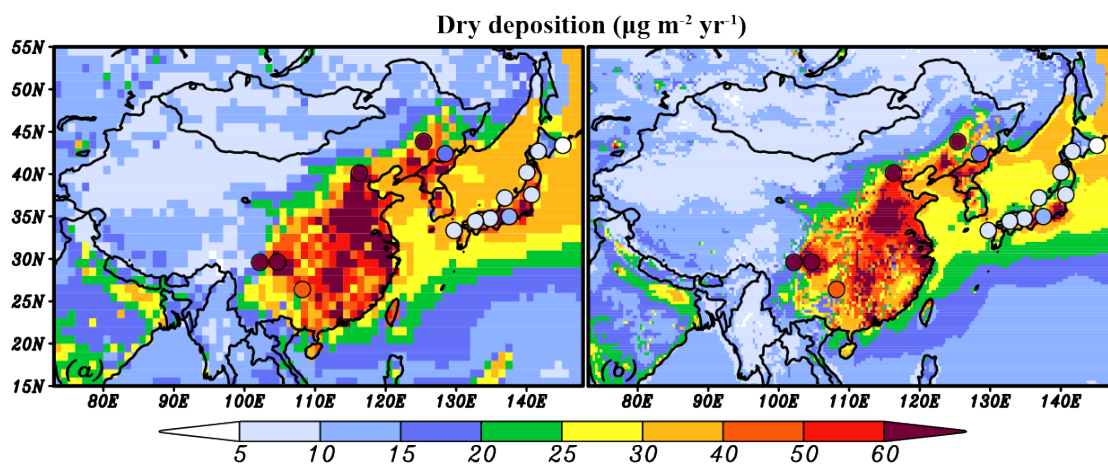


Fig. 9. Simulated annual mercury dry deposition ($\mu\text{g m}^{-2} \text{yr}^{-1}$) over East Asia in the global (a) and nested (b) domains in 2001. Overlaid points show observations collected from the literature. Note that observations and simulated results are not in the same year.

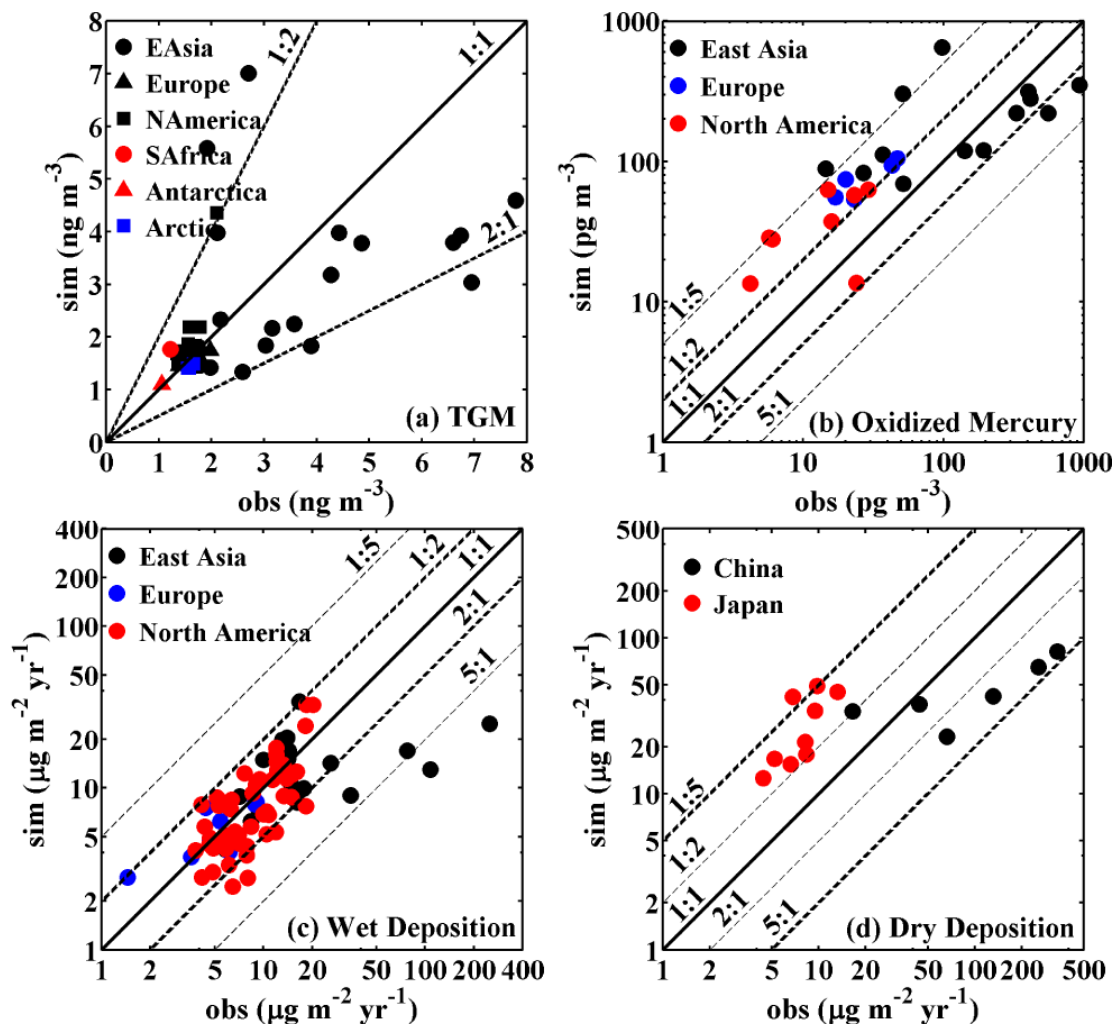


Fig. 10. Simulated vs. observed TGM (a), oxidized mercury (b), wet deposition (c), dry deposition (d) in different regions. Note that coordinates are different in different panels. Units of TGM, oxidized mercury, wet deposition and dry deposition are ng m^{-3} , pg m^{-3} , $\mu\text{g m}^{-2} \text{yr}^{-1}$, $\mu\text{g m}^{-2} \text{yr}^{-1}$, respectively.

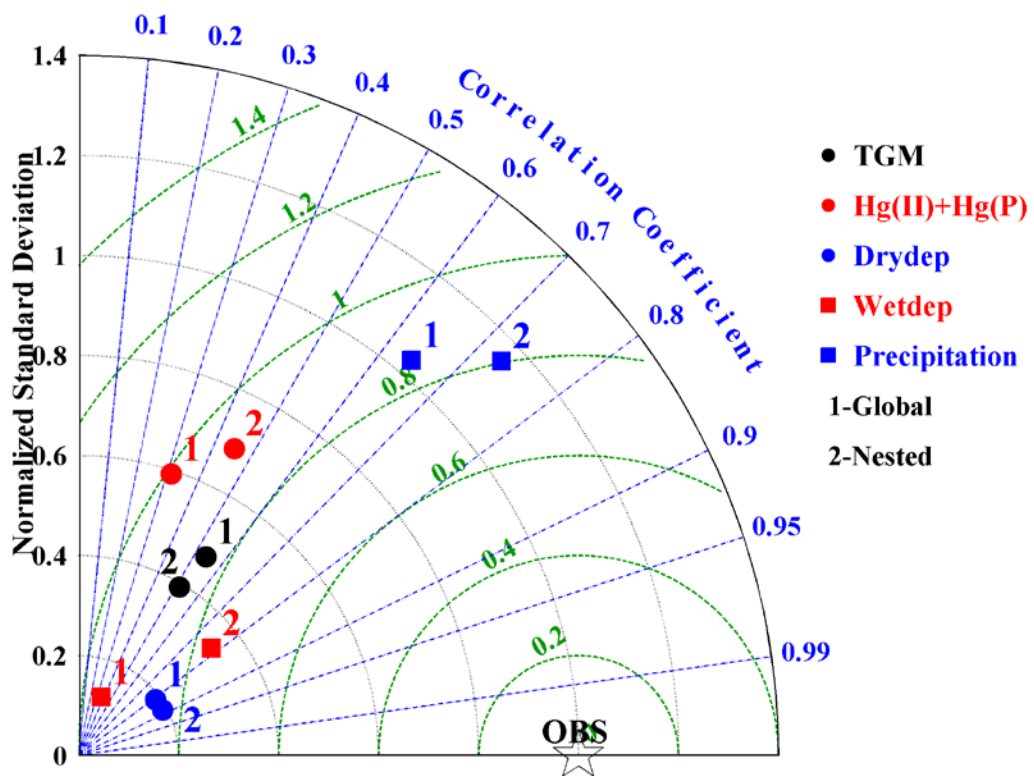


Fig. 11. Taylor Diagram of simulated annual TGM, Hg(II)+Hg(P), dry deposition, wet deposition and precipitation over East Asia in the global and nested domains (denoted by 1 and 2).

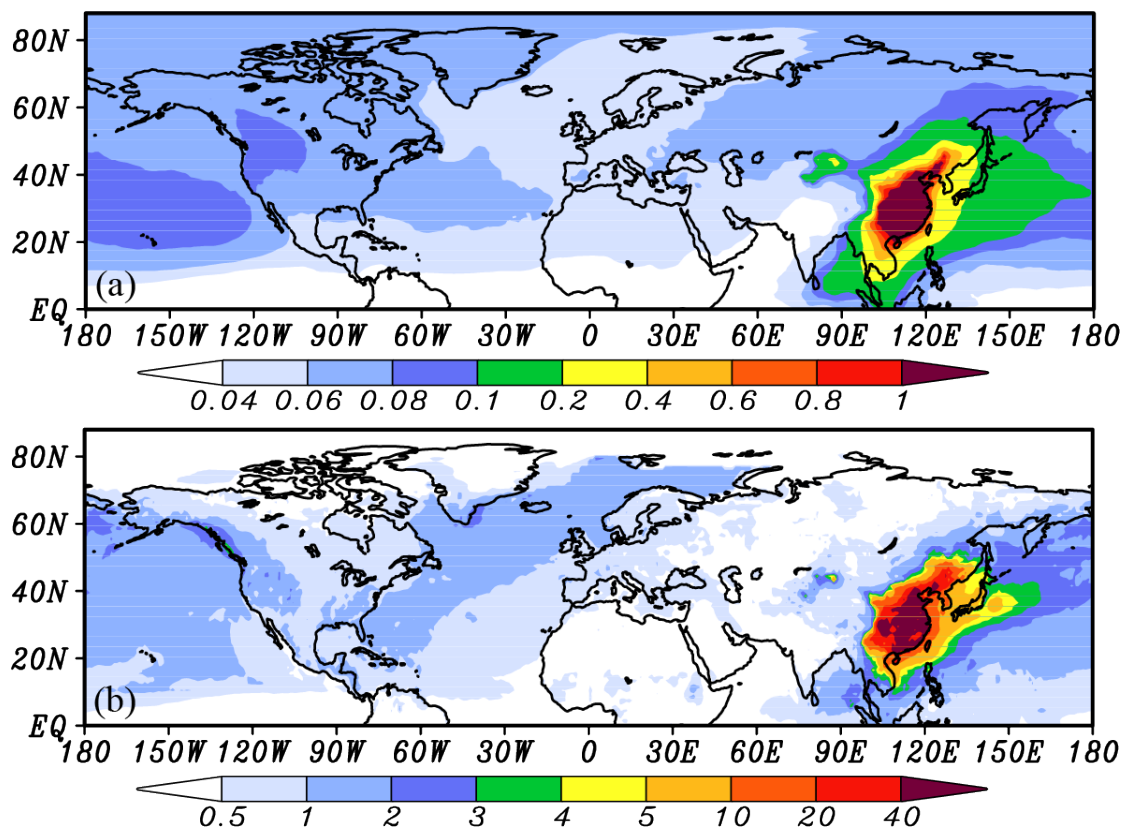


Fig. 12. Contributions of Chinese primary anthropogenic sources to (a) annual mercury surface concentrations and (b) total (wet plus dry) deposition in the Northern Hemisphere. The units of mercury concentrations and deposition are ng m^{-3} and $\mu\text{g m}^{-2} \text{yr}^{-1}$, respectively.

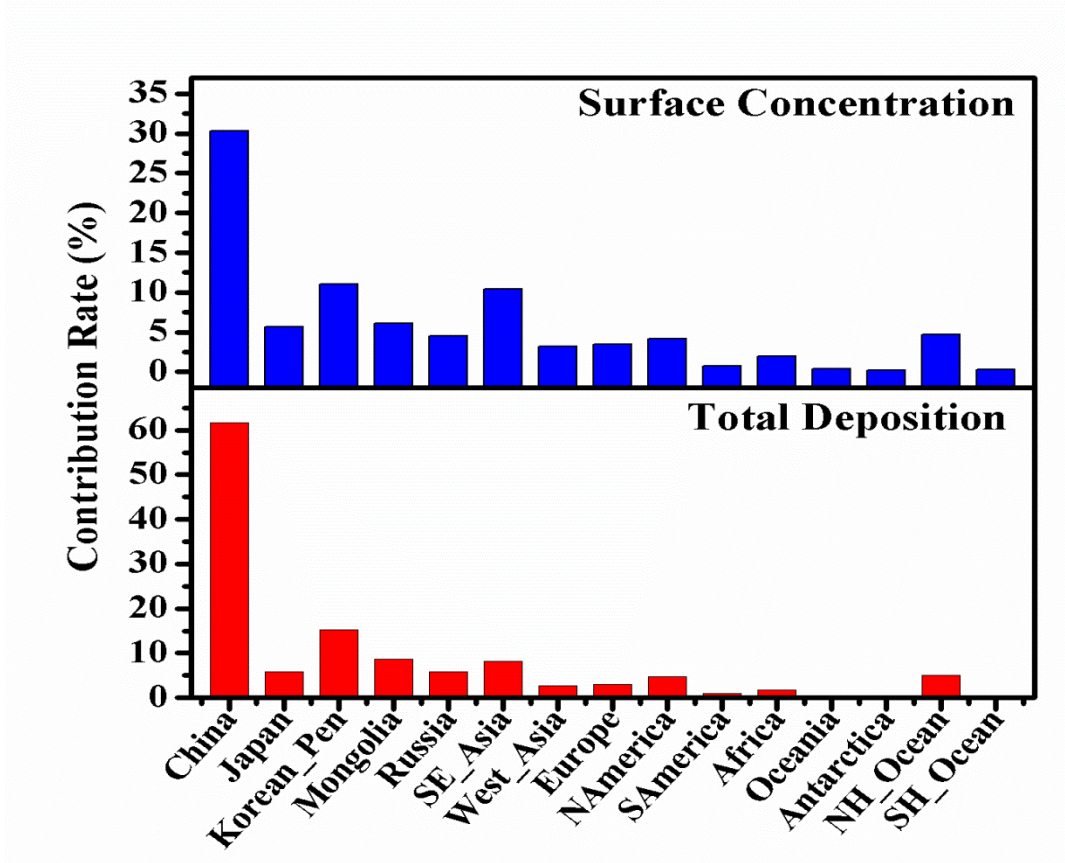


Fig. 13. Mean percentage contributions (%) from Chinese primary anthropogenic sources to annual mercury surface concentrations and total (wet plus dry) deposition over different world regions.